


Pyridoxine dehydrogenase SePdx regulates photosynthesis via an association with the phycobilisome in a cyanobacterium

Shoujin Fan^{1,†}, Wenzhe Li^{1,†}, Zhuo Chen^{1,†}, Zixu Wang¹, Xiang Cheng¹, Susu Zhang¹, Meixue Dai¹, Jinyu Yang², Leilei Chen^{2,*} and Guoyan Zhao^{1,*} 

¹College of Life Science, Shandong Normal University, Jinan 250014, China, and

²Institute of Agro-Food Science and Technology, Shandong Academy of Agricultural Sciences, Jinan 250100, China

Received 10 August 2024; revised 7 January 2025; accepted 27 January 2025.

*For correspondence (e-mail zhaoguoyan@sdu.edu.cn and chenleilei8210@163.com).

[†]These authors contributed equally to this work.

SUMMARY

Vitamin B6 (VitB6) deficiency is known to have a deleterious effect on photosynthesis, although the precise mechanism remains unclear. Pyridoxine dehydrogenase is a key protein involved in VitB6 biosynthesis, which facilitates the reversible reduction of pyridoxal (PL) and the oxidation of pyridoxine (PN), thereby contributing to VitB6 production. This study demonstrated the enzymatic activity of a pyridoxine dehydrogenase, SePdx, from the cyanobacterium *Synechococcus elongatus* PCC 7942 in the oxidation of PN. This protein is localized to the thylakoid membrane, interacts with components of the phycobilisome (PBS) and photosystem I (PSI), and plays a role in general stress responses. Deletion of *sepxd* leads to a distorted thylakoid membrane, shorter membrane spacing distances, and decreased phycobiliprotein content. Protein–protein interaction studies revealed interactions among SePdx, phycobiliprotein CpcA, and the PSI subunit PsaE. The structural analysis identified key residues that mediate SePdx–CpcA and SePdx–PsaE interactions, which were further confirmed through site-directed mutagenesis. Overall, the findings suggested that SePdx may influence PBS assembly, thereby establishing a link between VitB6 biosynthesis and photosynthesis.

Keywords: *Synechococcus elongatus* PCC 7942, pyridoxine dehydrogenase, phycobilisome, photosynthesis, VitB6 biosynthesis.

INTRODUCTION

Vitamin B6 (VitB6) biosynthesis is linked to photosynthesis, although the exact relationship remains unclear. Both microorganisms and plants can synthesize VitB6 through *de novo* and pyridoxal 5'-phosphate (PLP) salvage biosynthetic pathways (Mangel et al., 2019; Tambasco-Studart et al., 2005; Vanderschuren et al., 2013). The PLP and its analogs, which contain an aldehyde in the fourth position of the pyridine ring, support photosynthetic phosphorylation and exogenous cytochrome reduction (Black & Pietro, 1968). Havaux et al. (2009) observed that an Arabidopsis mutant deficient in VitB6 due to the deletion of the pyridoxal synthase gene *pdx1.3* exhibited reduced chlorophyll content and increased sensitivity to high light intensity and photo-oxidative stress (Havaux et al., 2009). The reduction in chlorophyll content was correlated with a decline in the abundance of light-harvesting complex II (LHCII), a peripheral antenna that plays a crucial role in

transferring energy to the reaction centers of photosystem II (PSII) (Havaux et al., 2009). Nonetheless, limited data are available on the association between VitB6 and photosynthesis, and the precise mechanisms through which they interact have yet to be fully elucidated.

In cyanobacteria, phycobilisome (PBS) serves as the functional equivalent of plant LHCII. The PBS is attached to the stromal side of the thylakoid membrane, filling most of the space between individual thylakoids. The PBS comprises bilin-bound phycobiliprotein and linker proteins (Adir, 2005; Watanabe & Ikeuchi, 2013), which generally form trimers of heterodimers $[(\alpha\beta)_3]$ and then hexamers $[(\alpha\beta)_3]_2$, stacking into rod-like structures with the help of the linker proteins (Adir, 2005; Yu & Glazer, 1982). High-resolution crystallographic structures of PBS in *Synechococcus elongatus* PCC 7942 (*Synechococcus* from here on) have been solved, showing a unique loose allophycocyanin (APC, $\lambda_{\max} = 652$ nm) hexamer and a canonical

phycocyanin (PC, $\lambda_{\max} = 620$ nm) hexamer, whereas it did not further assemble into rods (Marx & Adir, 2013; Nield et al., 2003). The PC from *Synechococcus* measures 110 Å in diameter and 60 Å in thickness, with its α and β subunits encoded by the *cpcA* and *cpcB* genes (Marx & Adir, 2013; Nield et al., 2003). In addition to the phycobiliproteins and linker proteins, several other proteins have recently been reported to participate in stabilizing PBS proteins and regulating PBS attachment to photosystem I (PSI) and PSII. These include ferredoxin-NADP⁺ reductase, immunophilin, molecular chaperone, and chlorophyll-binding proteins (Havaux et al., 2005; Liu et al., 2019; Sato et al., 2010; Yadav et al., 2022). However, the specific functions of many of these proteins remain poorly understood.

Pyridoxine dehydrogenase (Pdx, EC 1.1.1.65), also called NADPH-dependent pyridoxal reductase, plays a crucial role in the VitB6 biosynthesis pathway. This enzyme efficiently facilitates the reversible conversion of pyridoxal (PL) to pyridoxine (PN) and catalyzes the initial reaction in the salvage pathway (Herrero et al., 2011; Ito & Downs, 2020). Disruption of the *pdx* gene has been observed to impact vitamer levels and the osmotic stress response significantly (Herrero et al., 2011; Morita et al., 2004). Most cyanobacteria, including *Synechococcus*, do not rely on VitB6 supplementation for their growth, indicating that they may encode complete biosynthetic pathways for this essential compound. Conservation of *Escherichia coli* PLP biosynthesis enzymes PdxA, PdxJ, and PdxH have been observed in cyanobacteria (Mills et al., 2020). However, the investigation of VitB6 biosynthesis pathways in cyanobacteria remains unexplored (Mills et al., 2020). Similarly, the role of Pdx in cyanobacteria has not yet been characterized.

This study investigated the role of a pyridoxine dehydrogenase, specifically SePdx, derived from the cyanobacterium *Synechococcus elongatus* PCC 7942. The findings demonstrated that the activity of SePdx is involved in the oxidation of PN and interacts with the α -chain of PBS and PSI, thereby influencing the composition of thylakoid membrane components. The enzyme also plays a vital function in the growth and stress tolerance of cyanobacteria.

RESULTS

The gene encoding by *SYNPCC7942_RS00135* is a GreenCut2 pyridoxine dehydrogenase

The unannotated 35 kDa protein encoded by *SYNPCC7942_RS00135* from *Synechococcus elongatus* PCC 7942 (hereafter *Synechococcus*) showed high similarity (41.37% similarity; 90% coverage) to Arabidopsis pyridoxal reductase (AtPLR1) (Herrero et al., 2011). This gene is located in close proximity to the gene encoding denosylmethionine-8-amino-7-oxononanoate aminotransferase (*SYNPCC7942_RS00160*) within the class-III PLP-dependent aminotransferase family (Figure 1). The VitB6 biosynthesis pathway in *Synechococcus* has not been fully elucidated. This study mapped the VitB6 biosynthesis pathway in *Synechococcus* by comparing it with the VitB6 biosynthesis pathways in plants (Raschke et al., 2011) and analyzing orthologous proteins (Figure 1; Figure S1). Hypothetically, *SYNPCC7942_RS00135* catalyzes the reversible conversion of PN to PL (Figure 1).

To further confirm the function of *SYNPCC7942_RS00135* *in vivo*, a knockout mutant strain was generated by replacing the gene with a kanamycin cassette (Figure S2). After several rounds of dilution, the homozygous mutant strains were segregated. Liquid chromatography-mass spectrometry (LC-MS) profiling revealed a significant reduction of 49.3% in the amount of PL in the knockout lines compared with the wild-type (WT) strain, while the amount of PN showed a non-significant decrease of 13.4% (Figure 1; Figure S2). To further investigate the pyridoxine dehydrogenase activity of the protein *in vitro*, the gene responsible for coding was cloned into a pMBP_C vector and was heterogeneously expressed in *Escherichia coli* Rosetta 2(DE3). The enzymic reaction was initiated by the addition of PN, and the resultant production of PL was quantified through a reaction with phenylhydrazine. The data obtained revealed that the production of PL was significantly elevated in comparison to the control setup, which expressed the empty vector (Figure 1). These findings suggested that *SYNPCC7942_RS00135* catalyzes PN oxidation; therefore, it is referred to as SePdx, a pyridoxine dehydrogenase from *Synechococcus elongatus*.

Figure 1. The protein SePdx encoded by *SYNPCC7942_RS00135* is a pyridoxine dehydrogenase.

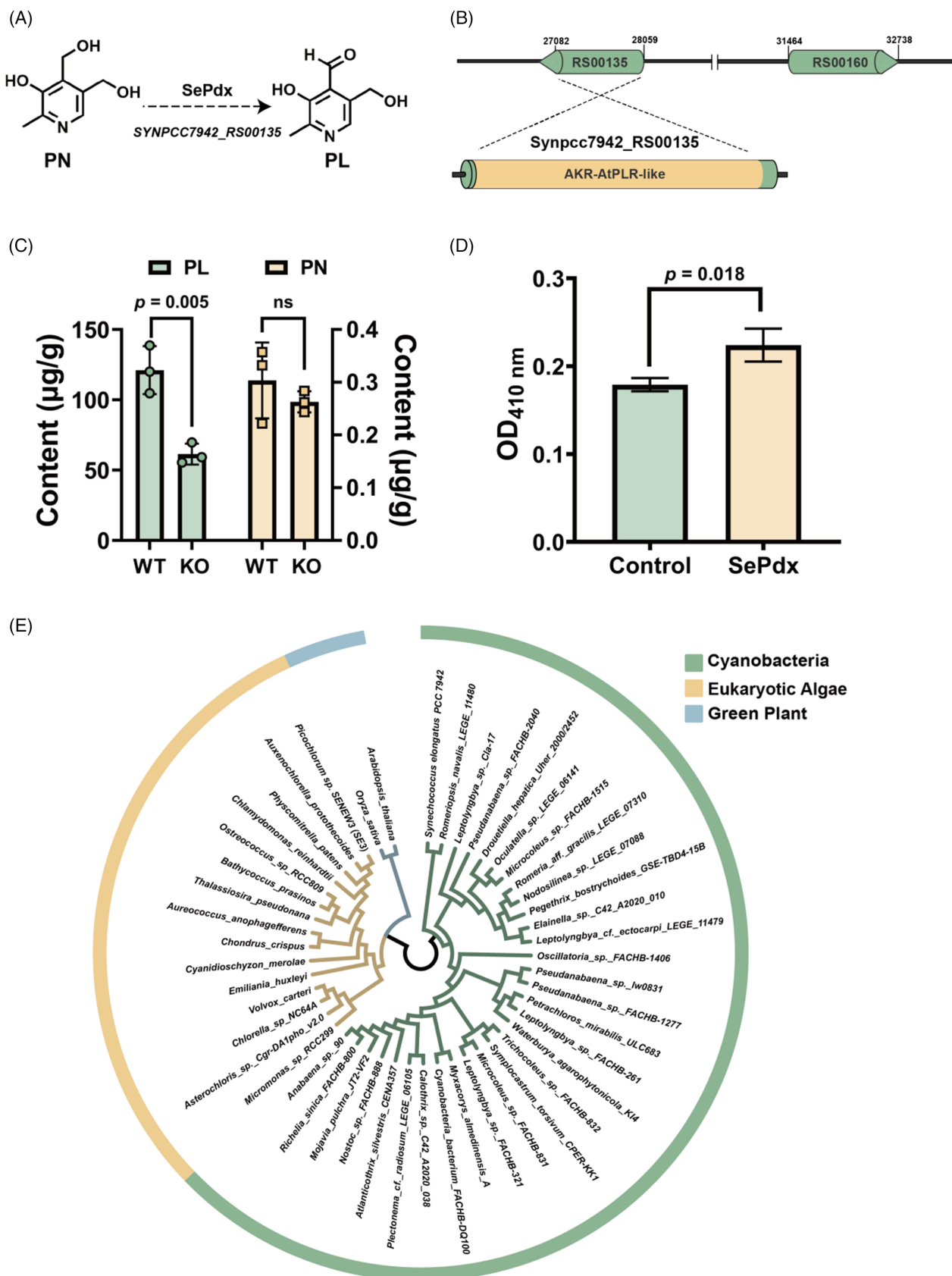
(A) SePdx catalyzes the conversion of PN to PL.

(B) Domain architecture of SePdx. The conserved domain was extracted from the NCBI database (CDD). The positions of *SYNPCC7942_RS00135* and *SYNPCC7942_RS00160* in the *Synechococcus* genome.

(C) The content of PL and PN in WT (green) *Synechococcus* and the $\Delta sepx$ mutant (yellow) strains, as detected by LC-MS. The mean and standard deviation (SD) of three independent experiments are reported, and *P*-values were determined using Student's *t*-test, with a significance threshold set at *P* < 0.05.

(D) The pyridine dehydrogenase activity of recombinant SePdx expressed in *Escherichia coli* Rosetta 2 (DE3). The production of PL was quantified by measuring the OD410 nm values following the addition of phenylhydrazine. The recombinant SePdx demonstrated a significant increase in PL production compared to the control. The mean and standard deviation (SD) of three independent experiments are reported, and *P*-values were determined using Student's *t*-test, with a significance threshold set at *P* < 0.05.

(E) Phylogenetic tree for SePdx-like protein sequences, as described in the "Materials and Methods" section (Dataset S1). Taxa are represented by color-coded strips: green for cyanobacteria, yellow for microalgae, and blue for plantae.



The phylogenetic tree demonstrated that SePdx is conserved in cyanobacteria, algae, and plantae but is evolutionarily distant from homologous proteins in non-photosynthetic organisms (Figure 1; Figure S3; Dataset S1). This finding aligned with the study by Karpowicz et al. (2011), which indicated that SYNPCCT942_RS00135 is a GreenCut2 protein (Karpowicz et al., 2011). SignalP did not predict a putative signal sequence (Sec/SPI). Spoctopus (<http://octopus.cbr.su.se/index.php>) predicted a transmembrane (TM) domain between amino acids 202 and 219. Additionally, Cello (<http://cello.life.nctu.edu.tw/>) identified SePdx as a membrane protein. The predicted structure of SePdx by AlphaFold2 (v2.0) (<https://github.com/deepmind/alphafold>) is primarily helical, consisting of 10 α -helices ($\alpha 1$ – $\alpha 10$), three short 3 $_{10}$ -helices ($\eta 1$ – $\eta 3$), and nine β -strands ($\beta 1$ – $\beta 9$). It exhibits a classical (α/β) 8 triosephosphate isomerase (TIM) barrel fold of pyridoxine dehydrogenase, with most of the protein in the N-terminal region, a small C-terminal β -sheet capping the TIM barrel, and two additional α -helices outside the barrel. The SePdx structure was also validated using DeepMSA2 analysis (<https://seq2fun.dcmf.med.umich.edu/DMFold>). While AlphaFold2 and DeepMSA2 models showed slight differences in $\alpha 10$ and $\beta 3$, they demonstrated significant structural similarities with a root mean square deviation (RMSD) of 0.37 Å (Figure S4).

Therefore, SePdx is a cyanobacterial pyridoxine dehydrogenase that is most likely localized on a membrane. Its evolutionary conservation suggested that the presence of SePdx has been positively selected in the green clades. Further studies should focus on elucidating the molecular mechanism by which SePdx influences cellular processes.

The *Δsepdx* mutant is sensitive to oxidative and salinity stresses

The growth of *Δsepdx* and WT strains was compared in BG-11 liquid medium at 30°C and 40 $\mu\text{mol photons m}^{-2} \text{sec}^{-1}$. The mutant did not show significant growth differences when measuring the OD730 nm values (Figure 2). However, the *Δsepdx* mutant cells exhibited impaired chlorosis reaction throughout all growth phases, in contrast to the green color of the WT strain (Figure 2). *Synechococcus* cells (day 8, OD730 nm = 1.5) were stained with Hoechst 33342 and PI. Hoechst 33342 stains live cells by penetrating the cell membrane, while PI selectively stains dead cells as it cannot pass through intact cell membranes. The findings revealed that *sepdx* deletion caused a significant increase in cell death compared to the WT control under normal conditions (Figure S5), which aligned with the observed yellow color of the mutant cells. A complemented strain *Δsepdx::psbA-sepdx* was generated by reintroducing a copy of the *sepdx* gene to the *Δsepdx* mutant under the control of the constitutive *psbA* promoter on plasmid pSyn_6. The green color was restored in the complemented mutant (Figure 2; Figure S5).

As VitB6-deficient plants have shown increased sensitivity to stress responses (Havaux et al., 2009), this study analyzed whether SePdx is essential for cyanobacteria to tolerate oxidative and salt stresses. In the presence of 5 mM H_2O_2 , the growth rate of *Δsepdx* mutant was severely affected (Figure 2B), and the cells appeared visually yellow (Figure 2C). Under the salinity condition (0.3 M NaCl), *Δsepdx* lines exhibited a lower survival rate than that of WT strains and showed a bleaching phenotype (Figure 2C, D). The stress-sensitive phenotypes were partially rescued by complementation (Figure 2D). Exogenous PL (0.3 μM) was added to the growth medium to determine whether the growth defects and stress-sensitive phenotype of *Δsepdx* were caused by the low amount of PL in the mutant. However, the supplementation of PL did not rescue the chlorosis and stress-sensitive phenotype of the mutant (Figure 2A,B,D), indicating that the lack of VitB6 is not the critical factor in determining the response of the *Δsepdx* mutant to stress. Additionally, the *Δsepdx* mutant displayed a higher survival rate than the WT strain under high light (150 $\mu\text{mol photons m}^{-2} \text{sec}^{-1}$) and nitrogen-starved (no nitrate) conditions (Figure 2E,F).

The *Δsepdx* mutant exhibits aberrant cell morphology and disorganized thylakoid membrane

Transmission electron microscopy (TEM) analysis revealed that the *Δsepdx* mutants exhibited altered cell morphology compared with WT cells. The thylakoid membrane appeared to be an intact and well-organized structure in WT cells, whereas it was disrupted in mutants. Specifically, the thylakoid membrane in the *Δsepdx* mutants appeared less distinct, with a lighter lumen than that in the WT strains (Figure 3A). It was observed that certain dense particles were missing from the mutant thylakoid membrane, a feature that was restored in the complementation lines (Figure 3A). These dense particles are most likely aggregates of photosynthetic light-harvesting complexes known as PBSs, with a typical diameter of approximately 30 nm on the stromal surfaces of the thylakoid membranes (Elanskaya et al., 2018). Measurements of thylakoid membrane spacing distances in TEM images indicated that the *Δsepdx* mutants displayed a significantly lower average spacing distance ($50.75 \pm 5.05 \text{ nm}$) than the WT cells ($57.26 \pm 4.49 \text{ nm}$) under the same growth conditions (Figure 3C). However, due to the limitations in the resolution of the thin sections, further isolation and analysis of PBSs are required to confirm this observation.

Additionally, the TEM analysis revealed that the cell length of the *Δsepdx* mutants was significantly shorter than that of the WT strains (Figure 3B). Microscopy observations further supported these results. During the early exponential phase (OD730 nm = 0.5), the average length of the long axis in the *Δsepdx* mutant cells was $1.50 \pm 0.39 \mu\text{m}$ ($n = 114$), whereas in WT cells, it

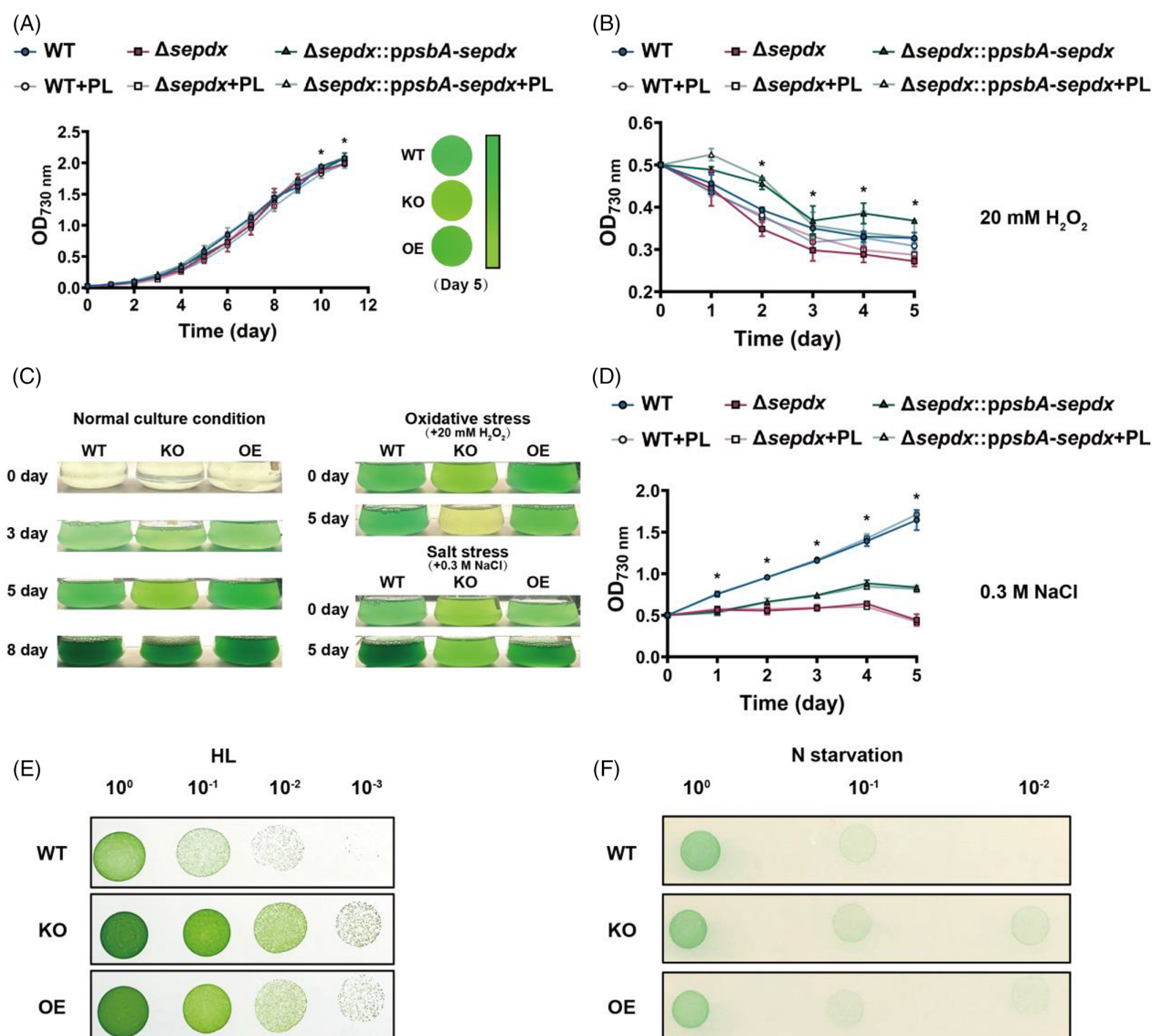


Figure 2. Impact of *sepdx* deletion on cell growth and stress tolerance.

(A) Cell growth curve of *Synechococcus* cells monitored over 11 days in normal BG-11 media under 40 μ mol photons m⁻² sec⁻¹ ($n = 3$). The initial OD_{730 nm} was 0.02.

(B) Effect of H₂O₂ (20 mM) on the growth of *Synechococcus* cells. The initial OD_{730 nm} was 0.5.

(C) Images of *Synechococcus* cell cultures were captured under normal conditions on days 0, 3, 5, and 8, while images of the cell cultures under stress conditions were captured on days 0 and 5.

(D) Effect of NaCl (0.3 M) on the growth of *Synechococcus* cells. The initial OD_{730 nm} was 0.5.

(E) Images of *Synechococcus* cells spotted on BG-11 agar after 5 days of growth under high light illumination (HL, 150 μ mol photons m⁻² sec⁻¹).

(F) Images of *Synechococcus* cells spotted on BG-11 agar after 3 days of growth under normal light illumination (40 μ mol photons m⁻² sec⁻¹). WT, WT strain; $\Delta sepdx$ (KO), *sepdx* deletion mutant strain; $\Delta sepdx::ppsba-sepdx$ (OE), *sepdx* complementation strain; +PL, exogenous PL (0.3 μ M) was added to the growth medium. All data are based on three independent biological replicates ($n = 3$), and the results are presented as mean \pm standard error of the mean (SEM). Statistical significance of differences between groups was assessed using a two-tailed Student's *t*-test, with a significance threshold set at $*P < 0.05$.

was $2.02 \pm 0.41 \mu\text{m}$ ($n = 94$; Figure S5). During the late exponential phase (OD_{730 nm} = 1.0) the average length of the $\Delta sepdx$ mutant cells decreased by 5.35% compared with that of the WT cells. During the stationary phase (OD_{730 nm} = 1.5), the average length of the $\Delta sepdx$ mutant cells was 9.27% lower than that of the WT cells. In contrast, the cell diameter of the $\Delta sepdx$ mutant cells showed a

significant increase ($0.972 \pm 0.087 \mu\text{m}$, $n = 64$, OD_{730 nm} = 1.0) compared with the corresponding WT cells ($0.916 \pm 0.069 \mu\text{m}$, $n = 45$, OD_{730 nm} = 1.0, Figure S5). Quantification of cell area revealed that, during the early exponential phase (OD_{730 nm} = 0.5), the average area of the $\Delta sepdx$ mutant cells was 18.34% smaller than that of the WT cells (Figure S5). In contrast, during the stationary phase

(OD730 nm = 1.5), the average area of the $\Delta sepx$ mutant cells was 22.38% larger than that of the WT cells (Figure S5).

In summary, the analysis of $\Delta sepx$ mutant cells revealed significant alterations in the structure of the thylakoid membrane, which may be linked to the observed phenotype of altered cell size and heightened sensitivity to stresses. Given the numerous altered phenotypes caused by the deletion mutant, it raises curiosity about whether SePdx functions as a universal regulator within the cell.

SePdx regulates protein levels of the photosystem complexes at the post-transcriptional level

Transcriptomic analysis was conducted to investigate the impact of SePdx on gene expression regulation. Total RNA was extracted from $\Delta sepx$ and WT at their late exponential phases (OD730 nm = 1.0), resulting in the detection of 2650 transcripts from 2664 genes on the chromosome (Figure S6; Dataset S2). As predicted, the knockout mutant lacked *sepx* transcription, confirming successful gene deletion. Differential expression analysis revealed significant changes ($P < 0.05$) in only two unannotated genes (*SYNPCC7942_RS00070* and *SYNPCC7942_RS01590*) at the mRNA level. Notably, no significant changes were observed in the expression levels of genes involved in cell growth, survival, and pigment biosynthesis. Hence, the possibility that SePdx can act as a global regulator could be excluded.

However, proteomic analysis revealed significant differences in protein abundance between the $\Delta sepx$ knockout mutant and the wild-type strain. In the mutant, 749 proteins were upregulated, while 179 proteins were downregulated (Figure S6; Dataset S3). Notably, key enzymes in the vitamin B6 biosynthesis pathway, such as PdxK ($\log_2 = 0.66$), PdxH ($\log_2 = 1.06$), and PDX2 ($\log_2 = 1.81$), showed significant upregulation (Figure 3D). This suggests that the absence of SePdx may trigger compensatory upregulation of other enzymes in the vitamin B6 biosynthesis pathway to maintain intracellular vitamin B6 levels.

Furthermore, in the $\Delta sepx$ knockout mutant, the abundance of phycobiliprotein CpcB ($\log_2 = -0.65$) and phycobilisome linker polypeptides CpcH ($\log_2 = -1.44$) and CpcI ($\log_2 = -2.23$) was significantly reduced

compared to the wild-type strain. Various PSII subunits, including PsbB ($\log_2 = -0.60$), PsbU ($\log_2 = -0.83$), and PsbV ($\log_2 = -0.70$), were downregulated, while PsbF ($\log_2 = 1.21$) was upregulated. Additionally, the PSI-related subunit PsaD ($\log_2 = -1.47$) was downregulated (Figure 3D). These results suggest a specific role for SePdx in the post-transcriptional regulation of photosynthetic protein levels.

SePdx localizes to thylakoid membranes

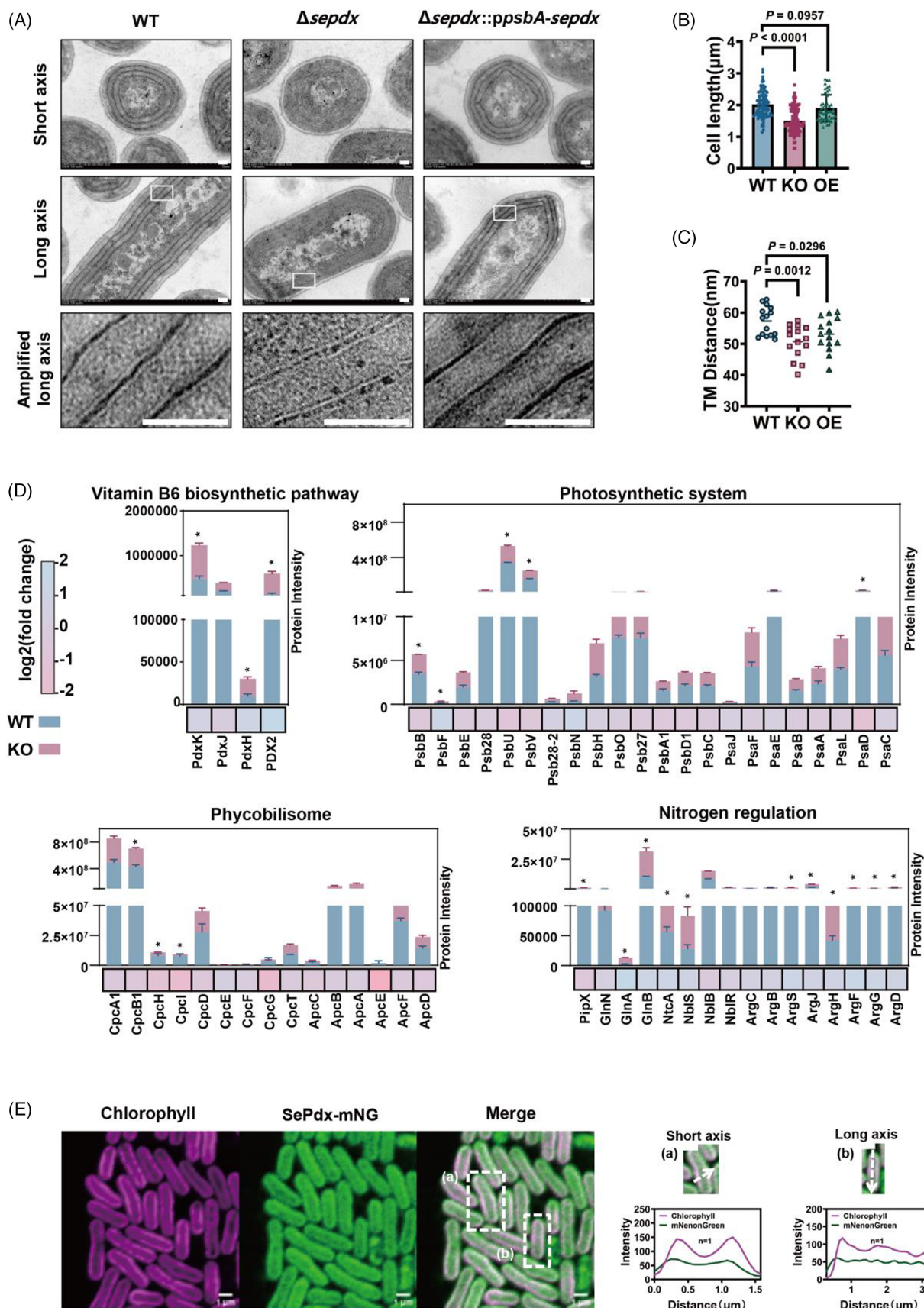
The changes in the thylakoid membrane of the mutant strain prompted an investigation into the subcellular localization of SePdx. To achieve this, the fluorescent protein mNeonGreen (mNG) and a 3×FLAG tag (DYKDDDDK) were fused to the C-terminus of SePdx, resulting in SePdx-mNG-FLAG. The FLAG was used for quality control and protein purification. The expression of the fusion protein was controlled by the *sepx* native promoter (Figure S7). Fluorescence signals from the SePdx fusion protein colocalized with chlorophyll autofluorescence signals on thylakoid membranes, as confirmed by image merging (Figure 3E). The detection of fluorescence on the thylakoid membrane also indicated that the function of SePdx is not compromised by the fused mNG and FLAG tags. These results suggested that SePdx localized to the thylakoid membrane rather than the cytosol, consistent with the predicted transmembrane domains in SePdx (Figure S4).

To confirm the localization of SePdx on the thylakoid membrane, the thylakoid membranes were isolated using sucrose gradient ultracentrifugation. Immunoblot analyses of crude and purified membrane fractions from *Synechococcus* showed that SePdx is associated with the thylakoid membranes (Figure S8). These observations support the hypothesis that SePdx is a thylakoid membrane-binding protein.

As the structure and fluidity of the thylakoid membrane are known to impact photosynthesis significantly, the modifications observed in the thylakoid membranes of $\Delta sepx$ cell, as well as the localization of the SePdx in the thylakoid membranes, suggested a possible additional role of *sepx* in regulating photosynthetic processes. Further research is needed to validate this hypothesis.

Figure 3. Impact of *sepx* deletion on cell morphology and subcellular localization of SePdx.

(A) Short-axis and long-axis TEM images of *Synechococcus* cells at an optical density of 1.0 at 730 nm. All scale bars are 100 nm.
 (B) The cell length of *Synechococcus* cells was measured using TEM images. The mean and standard deviation (SD) of three independent experiments are reported, and P -values were determined using Student's t -test, with a significance threshold set at $P < 0.05$.
 (C) Thylakoid membrane (TM) spacing distances as measured using TEM images. The mean and standard deviation (SD) of three independent experiments are reported, and P -values were determined using Student's t -test, with a significance threshold set at $P < 0.05$.
 (D) Comparison between the *sepx* knockout mutant (KO) and the wild-type (WT) strains in terms of protein abundance changes of vitamin B6 biosynthesis-related proteins, photosynthesis-related proteins, and nitrogen regulation-related proteins. The heatmap represents \log_2 (fold change), the bar graphs indicate relative protein abundance, and “*” denotes statistically significant differences ($P < 0.05$). Proteomic data are available in Dataset S3.
 (E) Intracellular localization of SePdx:mNG (green) in *Synechococcus* cells and its relationship with the thylakoid membrane (magenta). The first row: chlorophyll fluorescence; the second row: mNeonGreen emission; the third row: merged first and second rows. All scale bars are 1 μ m.



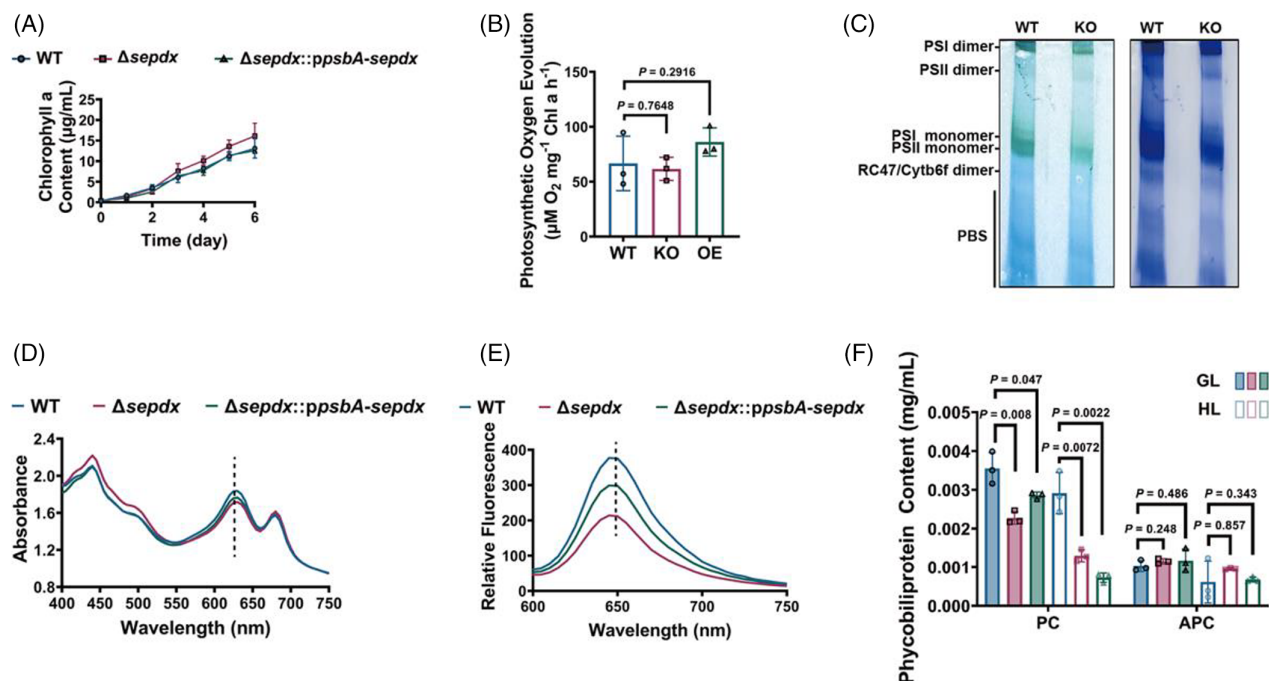


Figure 4. Impact of *sepdx* deletion on photosynthesis.

(A) Chlorophyll (Chl) *a* content of *Synechococcus* cells (OD730 nm = 1.0).

(B) Photosynthesis oxygen evolution analysis of the *Synechococcus* cells (OD730 nm = 1.0). Error bars represent \pm SD ($n = 3$).

(C) BN-PAGE of *Synechococcus* thylakoid membranes (OD730 nm = 1.0). Left: chlorophyll staining; right: Coomassie Blue staining.

(D) Absorption spectra of *Synechococcus* cells (OD730 nm = 1.0). The original absorption spectra were normalized at 750 nm.

(E) Fluorescence emission spectra of *Synechococcus* cells (OD730 nm = 1.0). The original fluorescence emission spectra were normalized at 750 nm.

(F) Phycobiliprotein contents of *Synechococcus* cells (OD730 nm = 1.0) under normal light (GL, 40 µmol photons m⁻² sec⁻¹) and high light conditions (HL, 150 µmol photons m⁻² sec⁻¹). PC, phycocyanin; APC, allophycocyanin. Error bars represent \pm SD ($n = 3$). KO ($\Delta sepdx$), *sepdx* deletion mutant strain; OE ($\Delta sepdx::ppsbA-sepdx$), *sepdx* complementation strain; WT, WT strain.

The $\Delta sepdx$ mutant affects the assembly of photosystem complexes

To explore the effect of *sepdx* on photosynthetic processes, chlorophyll content was first assessed using spectrophotometric analysis, as chlorophyll is one of the main pigments predominantly located in thylakoid membranes. The results indicated no significant difference in chlorophyll content between the $\Delta sepdx$ mutant and WT cells during growth (Figure 4A). Additionally, measurements of oxygen evolution revealed no statistically significant variations in PSII electron transfer rates between the WT and the $\Delta sepdx$ mutants, suggesting that the deletion of *sepdx* did not affect the PSII electron transfer rates of *Synechococcus* (Figure 4B).

Furthermore, Blue Native (BN)-PAGE analysis was conducted to assess the impact of the mutation on photosynthesis complex assembly. Thylakoid membranes from *Synechococcus* WT and $\Delta sepdx$ mutant cells were grown under 40 µmol photons m⁻² sec⁻¹. They were isolated and solubilized in 3% *n*-dodecyl β -D-maltoside. The analysis revealed that the abundance of the cytochrome *b₆f* complex and PSII remained unaffected in the mutant; however, the levels of PBS and monomeric PSI were reduced in

sepdx deletion mutant cells compared with the WT (Figure 4C).

SePdx is associated with phycobilisome proteins

Full-wavelength and fluorescence spectra of the *Synechococcus* cells were further investigated to study the effect of *sepdx* on the abundance of PBS. The mutant strain exhibited a significant decrease in phycocyanin content compared with the WT strain. The full-wavelength scan of WT (OD730 nm = 1.0) revealed lower absorption values at 620 nm, which is the peak absorption wavelength of phycobilisomes, in $\Delta sepdx$ mutant cells than in WT cells (Figure 4D). This observation was further supported by fluorescence spectra, which demonstrated a reduced fluorescence intensity at the 650 nm peak with 545 nm excitation in $\Delta sepdx$ cells compared with the WT (Figure 4E). These spectral findings along with the BN-PAGE results supported a decrease in phycobilisome content in the $\Delta sepdx$ mutant strain.

To further validate this hypothesis, phycocyanin and allophycocyanin were isolated from the phycobilisomes of *Synechococcus* cells. Under normal growth conditions at 40 µmol photons m⁻² sec⁻¹, the $\Delta sepdx$ mutant cells

exhibited a significant 35.90% reduction in phycocyanin content compared with the WT strain (Figure 4F). This reduction in the phycocyanin content in the mutant cells increased to 55.42% when exposed to high light conditions ($150 \mu\text{mol photons m}^{-2} \text{sec}^{-1}$) (Figure 4F). In contrast, there was no significant difference in allophycocyanin content between the Δsepx mutant and WT strains under normal or high light conditions. Therefore, deletion of the *sepx* gene specifically affects the content of phycobilisomes in *Synechococcus*, particularly in relation to phycocyanin content. The decreased phycocyanin content in the Δsepx mutant cells can account for the observed chlorosis and shorter thylakoid membrane spacing distances.

SePdx physically interacts with phycobilisome proteins

To gain further insight into the molecular mechanism of SePdx, affinity purification-mass spectrometry (AP-MS) experiments were performed using SePdx-mNG-FLAG cells. The cells ($\text{OD}_{730} = 1.0$) were lysed and resuspended in a buffer containing 10% digitonin to solubilize membrane proteins. The SePdx-mNG-FLAG and its interacting partners were isolated using anti-FLAG affinity resin and analyzed by mass spectrometry (MS). The pull-down samples exhibited a blue color reminiscent of the phycobilisome. A total of 338 proteins were identified in the replicates (Dataset S4). To address the limitation of distinguishing between direct and indirect interactions, protein-prey interactions were assessed using the weighted D-score (WD-score) and Z-score (Figure 5A, Dataset S4). Interactions with both the WD- and Z-scores in the top 5% were considered to have high reproducibility, specificity, and abundance (Mackinder et al., 2017). The cut-off value for the WD-score was determined to be 3.70 and that for the Z-score was 1.79 at the 95% confidence level. Eight interactions with SePdx-mNG-FLAG surpassed these thresholds, indicating high-confidence interacting proteins of SePdx (Figure 5A). Among these interactions, the top five proteins with the highest WD- and Z-scores included three phycobilisome components, CpcA1, CpcB1, and ApcB (Figure 5A), suggesting interactions between SePdx and phycobilisome proteins.

A bacterial adenylate cyclase two-hybrid assay (BACTH) was performed to confirm the interaction of SePdx with phycobilisome proteins *in vivo*. SePdx and its potential interacting partners were fused to the T18 and T25 fragments of adenylate cyclase in this assay. This interaction was assessed by monitoring the β -galactosidase activity employing *o*-nitrophenyl beta-D-galactopyranoside (ONPG) as the substrate. The results revealed a direct interaction between SePdx and CpcA1, while no interactions were detected with CpcB1, ApcA, or ApcB (Figure 5B,C). CpcA1 and CpcB1 are phycocyanin subunits, while ApcA and ApcB are subunits of allophycocyanin. This finding suggested that SePdx

specifically interacts with phycocyanin rather than allophycocyanin, which aligns with the observed impact of *sepx* gene deletion on phycocyanin levels but not allophycocyanin levels. Additionally, BACTH showed that SePdx directly interacted with the PSI core protein PsaE but did not interact with PSII subunits. Overall, the BACTH assay suggested that SePdx is associated with phycobilisomes, directly interacts with CpcA1, and potentially interacts with the PSI complex.

SePdx interacts specifically with the α -chain of phycocyanin

A more precise characterization of the interaction of SePdx and phycocyanin requires structural information. To achieve this, docking experiments were performed on the X-ray structure of the monomeric form of phycocyanin (PDB: 4H0M) (Marx & Adir, 2013) from *Synechococcus* and the AlphaFold2 model of SePdx. The flexible docking model (Figure 6A) perfectly matched the BACTH data, indicating that SePdx directly interacted with the α -chain of phycocyanin encoded by *cpcA1*. The refined structural data suggested that the SePdx-CpcA1 interaction was characterized by three hydrogen bonds and two electrostatic interactions with a ΔG score of -48 kcal/mol . A flexible region in the structure of SePdx was observed in the interaction interface, surrounded by Asp-28 and Tyr-31 from the loop downstream to $\beta 2$, Arg-189 from $\alpha 6$, and Gln-214 in a short 3_{10} helix ($\eta 2$). This region forms hydrogen bonds and salt bridges in association with the outermost helices of CpcA1. Moreover, Arg-96 from the turn downstream to $\beta 5$ of SePdx may contribute to the binding by electrostatic interaction with Asp-49 from the helix of CpcA1. Overall, by aligning the docking model with the hexamers of phycocyanin, it was observed that SePdx bound to the topmost portion of the phycocyanin via the interaction with CpcA1.

Site-directed mutagenesis was performed to examine the contributions of the residues in more detail. Residues Asp-28, Tyr-31, Arg-96, Arg-189, and Gln-214 of SePdx were individually mutated to Ala (D28A, Y31A, R96A, R189A, and Q214A). The resulting mutants were assessed for their interaction with CpcA1 by measuring β -galactosidase activity. Compared with WT SePdx, mutants D28A, Y31A, R96A, R189A, and Q214A showed decreased β -galactosidase activity by 67.6, 46.3, 65.1, 60.8, and 40.3%, respectively (Figure 6C). More importantly, all five mutants exhibited statistically significant differences from the WT protein ($P < 0.05$). These findings collectively indicated that SePdx binds directly to the α -chain of phycocyanin through hydrogen bonding and electrostatic interactions.

SePdx potentially interacts with PsaE

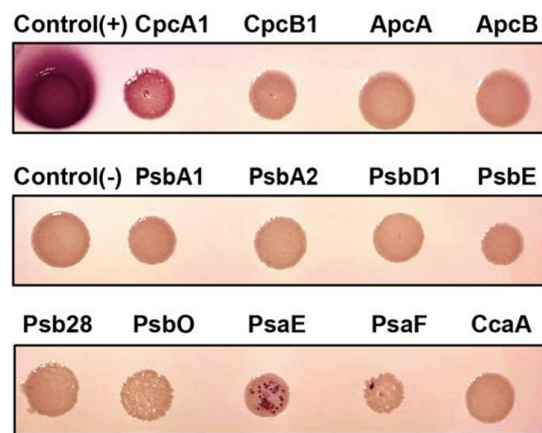
Docking experiments were also conducted to explore the potential interaction between SePdx and PSI using the X-ray structure of the PSI core subunit PsaE (PDB: 6KIG) (Cao

(A) Most abundant proteins identified by MS to interact with SePdx

Accession Number	Name	MW	Number of peptides		WD score	Z-score
			1	2		
SYNPCC7942_RS10995		18	1	2	18.00	2.04
SYNPCC7942_RS05370	CpcB1	18	62	103	9.08	1.81
SYNPCC7942_RS05375	CpcA1	17	69	80	8.63	1.80
SYNPCC7942_RS01660	ApcB	17	24	24	4.90	1.82
SYNPCC7942_RS03450	HemF	36	1	3	4.38	1.94
SYNPCC7942_RS04555	TufB	44	22	16	4.36	1.80
SYNPCC7942_RS05210		103	7	10	4.33	1.85
SYNPCC7942_RS04560	FusA	76	14	22	4.24	1.80

The experiment was performed in biological twice, indicated by the number 1 to 2. MW, molecular weight in kDa.

(B)



(C)

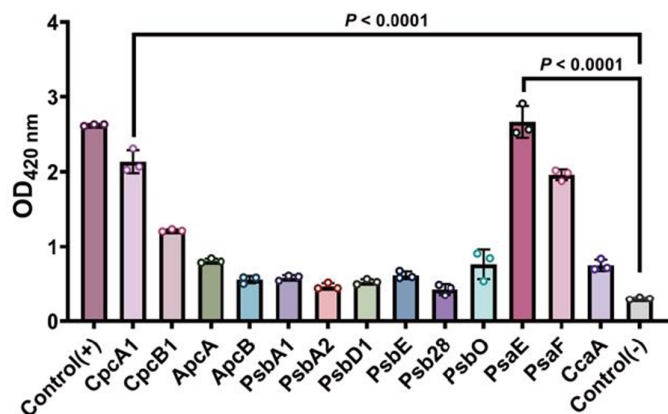


Figure 5. Protein–protein interaction study for SePdx. (A) High-confidence interaction proteins for SePdx identified from replicated AP-MS experiments using SePdx:FLAG cells. The complete sets of proteins from the AP-MS experiments are presented in Dataset S4. (B) Bacterial two-hybrid assays depicting the *in vivo* interaction between SePdx binding and potential interactors identified by AP-MS. In these assays, SePdx was fused to the T25 fragment of adenylate cyclase, while the interactor variants were fused to T18C. The proteins were tested for interaction with *E. coli* BTH101 cells cultured on MacConkey plates at 30°C for 3–5 days. Control (+), *E. coli* containing positive control vectors pKT25-zip/pUT18C-zip. Control (–), *E. coli* containing empty vectors pKT25/pUT18C. (C) The output from the two-hybrid system was detected as β -galactosidase activity. The mean and SD of three independent experiments are reported, and *P*-values were determined using Student's *t*-test.

et al., 2020). The docking model and structural data revealed three groups of residues involved in the formation of hydrogen bonds between SePdx and PsaE, resulting in a ΔG score of -360 kcal/mol (Figure 6B). Analysis of the interaction interface revealed that Thr-5, which is located in the flexible region of the SePdx initiation site, may form a hydrogen bond with Asn-47. Similarly, Gly-299, found in the flexible region following $\alpha 9$, may form a hydrogen bond

with Ser-52 of PsaE. Moreover, Tyr-144 in $\alpha 4$ of SePdx may contribute to the formation of a hydrogen bond with Ser-31 in PsaE. Alignment with the structure of the PSI complex (PDB: 6KIG) revealed that SePdx binds to the apical side of PsaE. Furthermore, the binding sites of PsaE and CpcA1 in the SePdx structure are opposite (Figure 7A).

Site-directed mutagenesis was performed to investigate the effect of specific residues on the interaction

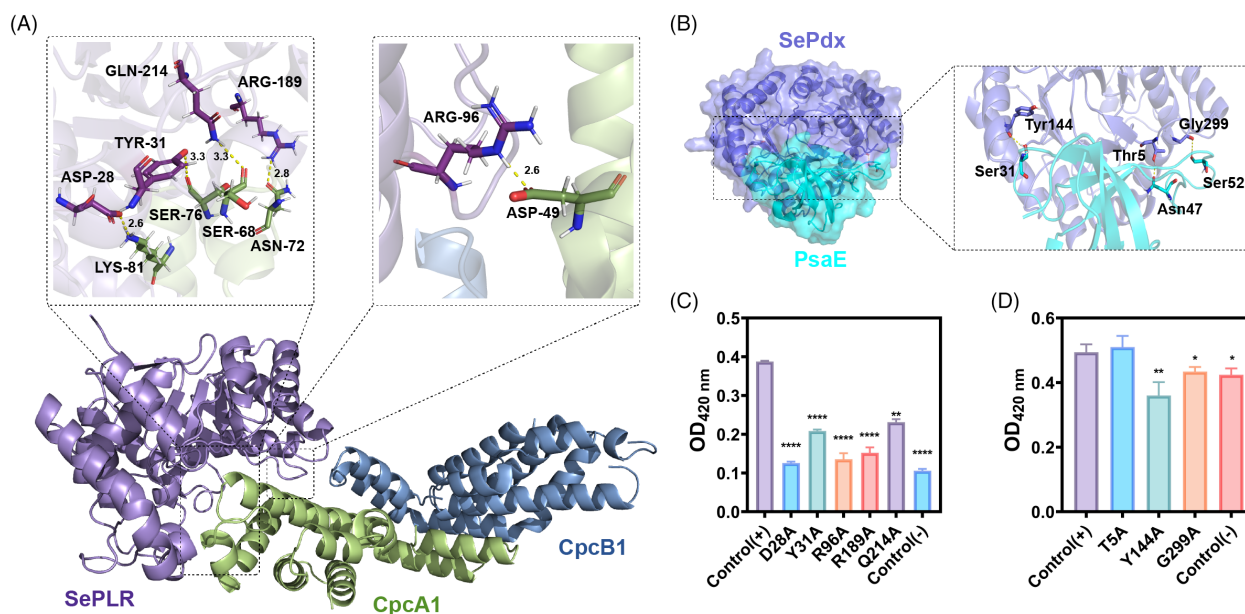


Figure 6. Structural model of the SePdx-phycoerythrin and SePdx-PsaE complex interactions.

(A) Docking model of the SePdx-phycoerythrin complex. The cartoon structures show SePdx in purple, CpcA (PDB: 4H0M) in green, and CpcB (PDB: 4H0M) in blue. The binding poses of SePdx-phycoerythrin are shown in an expanded view, with the binding sites and common binding residues shown in stick mode.

(B) Docking model of the SePdx-PsaE complex. The cartoon structures represent SePdx in purple and PsaE (PDB: 6KIG) in cyan. The binding pose of SePdx-PsaE is displayed in an expanded view, and the binding sites and common binding residues are shown in stick mode.

(C) Critical residues responsible for SePdx-phycoerythrin interaction identified through site-directed mutagenesis. The β -galactosidase activities were determined. Control (+), *E. coli* containing positive control vectors pKT25-zip/pUT18C-zip. Control (-), *E. coli* containing empty vectors pKT25/pUT18C. The mean and standard deviation (SD) of three independent experiments are reported, and *P*-values were determined using Student's *t*-test, with a significance threshold set at *P* < 0.05. * indicates *P* < 0.05, ** indicates *P* < 0.01, **** indicates *P* < 0.0001.

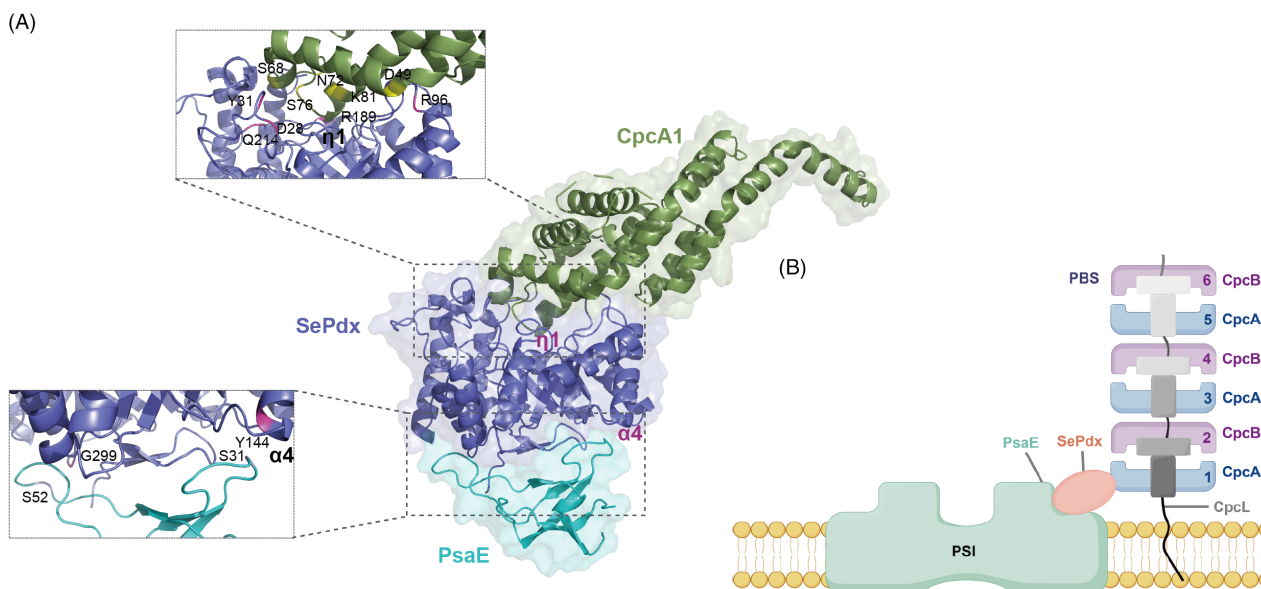


Figure 7. Model of SePdx in photosystem complex and hypothetical functional models.

(A) Alignment of SePdx in the SePdx-CpcA and SePdx-PsaE complexes. The binding poses are presented in the expanded views. The cartoon structures show SePdx in purple, CpcA (PDB: 4H0M) in blue, and PsaE (PDB: 6KIG) in cyan.

(B) Hypothetical model for the positioning of SePdx on/in the thylakoid membrane. The information on the PSI dimeric and PBS structures was used to create the model (Zheng et al., 2021). The red circle indicates that the SePdx would fit into the cavity between the PBS and PSI according to the proposed functional model.

between SePdx and PsaE. Mutants T5A, Y144A, and G299A were generated by replacing Thr-5, Tyr-144, and Gly-299 in SePdx with Ala. The interaction of these mutants with PsaE was evaluated by measuring β -galactosidase activity. Mutants Y144A and G299A exhibited 27.16 and 12.19% decreases in β -galactosidase activity, respectively, compared with WT SePdx. In comparison, Thr-5 showed a 3.19% increase (Figure 6D). Notably, only mutants Y144A and G299A exhibited statistically significant differences ($P < 0.05$) from the WT protein. These findings indicated that SePdx likely interacts with PsaE through hydrogen bonding.

DISCUSSION

SePdx is a pyridoxine dehydrogenase with an AKR_AtPLR-like domain and a predicted transmembrane domain (Figure 1; Figure S4). Fluorescent imaging data disclosed that SePdx is localized in the thylakoid membrane or is at least attached to it. Western blotting further confirmed this localization in the thylakoid membrane purified by sucrose gradient ultracentrifugation. The localization pattern of SePdx is consistent with its homologous proteins, Slr0545 (56.91% identity) and Slr1503 (42% similarity), from *Synechocystis* sp. PCC 6803, which is also found in the fractions of the low-density plasma membrane and thylakoid membrane (Wang et al., 2022). This suggested that SePdx may be involved in specific physiological processes associated with the thylakoid membrane. Moreover, phylogenetic analysis indicated that SePdx and its homologous proteins are clustered to the green lineage, spanning from cyanobacteria to algae and higher plants, and are distant from the proteins found in heterotrophic/chemoautotrophic bacteria, fungi, or mammals. These findings are in line with those of Rubin et al. (2015), who classified the coding gene (*Synpcc7942_RS00135*) of SePdx within the GreenCut2 genes (Heinrich & Grossman, 2013; Karpowicz et al., 2011), implying a specialized function of the pyridoxine dehydrogenase SePdx in photosynthetic organisms.

Previous studies have shown a relationship between vitamin B6 biosynthesis and photosynthesis in algae and plants, with implications including decreased efficiency of the light-harvesting complex, increased light sensitivity, compromised production of photosynthetic pigments, and the localization of vitamin B6 synthase in chloroplasts (Havaux et al., 2009; Raschke et al., 2011; Rueschhoff et al., 2013; Sang et al., 2011; Tambasco-Studart et al., 2007). Our study demonstrates that SePdx links VitaB6 biosynthesis to photosynthetic complex assembly by interacting with the α -chain of PBS encoded by *cpcA1*. First, SePdx demonstrates enzymatic activity in oxidizing PN, as confirmed by knockout and biochemical assays. Second, SePdx is involved in photosynthesis, as shown by the chlorosis and altered protein levels of photosystem complexes in *sepx* deletion mutant cells. Notably, we utilized the

commercial plasmid pSyn_6 to complement the *sepx* gene by integrating it into the neutral site NS1. The system employed a *psbA* promoter of relatively short length (222 base pairs) to regulate gene expression. However, this promoter may lack sufficient transcriptional activation capacity, potentially resulting in inadequate expression of the target gene and affecting the restoration of the original phenotypes.

The dual function of SePdx may be attributed to its binding capacity with PBSs, supported by AP-MS and BACTH experiments. Consequently, deletion of *sepx* causes a reduced electron density of the thylakoid membrane system, and a shorter membrane spacing than WT cells, suggesting truncation of electron-dense PBSs that hinders direct interaction of thylakoid membranes. The fluorescence spectrum and isolation of PBS further support the role of SePdx in maintaining PBS assembly. Similarly, Havaux et al. (2009) demonstrated in *Arabidopsis* that the absence of the pyridoxal synthase gene *pdx1.3* leads to a decrease in the quantity of LHCII, an essential light-harvesting complex in plants similar to PBS in cyanobacteria. Under stress conditions, PBS constituents are often degraded to reallocate available nitrogen for essential growth and survival functions (Krauspe et al., 2021). Degradation generally starts at the distal phycocyanin rods and progresses to the allophycocyanin core (Hu et al., 2020). The *sepx* deletion mutant with reduced phycocyanin content can not contribute available nitrogen as effectively as the WT strain, and this deficiency could not be compensated by additional PL. However, The reduced antenna size of PBS can improve the light-to-biomass conversion efficiency in *Synechococcus* cultures, allowing the cyanobacterium to prevent excess light energy absorption and evade photoinhibition and photodamage caused by high light intensity (Ungerer et al., 2018), thereby conferring stronger growth capacity to the $\Delta sepx$ mutant under high light and nitrogen-deprivation conditions.

One possibility is that SePdx regulates PBS by influencing nitrogen metabolism. PLP, the active form of VitB6, is an essential coenzyme involved in amino acid metabolism (di Salvo et al., 2011). The PL content was significantly altered in the *sepx* deletion mutant compared with the WT, potentially impacting the levels of PLP (the phosphorylated form of PL) and subsequently affecting the nitrogen status. PBS serves as a nitrogen store and degrades under nitrogen-starved conditions to release amino acids as nitrogen sources (Richaud et al., 2001). Disruption in PLP homeostasis can impact PBS biosynthesis. This suggested that the function of SePdx is similar to that of PipY in *Synechococcus* (Labella et al., 2017) and PDX3 in *Arabidopsis thaliana* (Colinas et al., 2016; Zheng et al., 2023), both of which are involved in PLP homeostasis and play conserved roles in VitB6 and amino/keto acid homeostasis. Additionally, our proteomic analysis revealed

that SePdx deletion significantly altered the abundance of proteins linked to the nitrogen regulatory network. However, our results indicated a specific effect of SePdx on phycocyanin rather than allophycocyanin, which leaves the association mechanism between SePdx and specific phycocyanin unexplained.

Another model based on protein interaction data would include SePdx in the assembled structure between the PBS and the PSI (Figure 7B). Cyanobacteria have two types of PBS: the large CpcG-PBS, with a typical core and peripheral rods, and the small CpcL-PBS, which lacks an allophycocyanin core and consists of a single phycocyanin rod assembled by linker proteins and anchored to thylakoid membranes by CpcL (Kondo et al., 2005, 2007, 2009; Watanabe et al., 2014; Zheng et al., 2023). The small PBS is associated with PSI, directly transferring energy to PSI without the core structure (Zheng et al., 2021); however, the interaction between these two complexes is poorly understood. This model proposed that the membrane-anchored SePdx can stabilize the small PBS and PSI by interacting with CpcA and PsalE. Consistently, the docking structure indicated that CpcA and PsalE bind at opposite sites in the SePdx structure. Notably, PsalE exposes a domain toward the cytoplasm, which may facilitate the binding of SePdx (Kato et al., 2019). This hypothesis is supported by the fact that deletion of *sepxd* does not affect PSII oxygen evolution or allophycocyanin function. This model suggested a functional role for SePdx comparable to that of the cyclophilin anaCyp40, which connects the large PBS and PSI by binding to ApcA and PsalE (Yadav et al., 2022). However, the precise mechanism of this regulatory function remains unclear at this stage, requiring further investigation for a comprehensive understanding.

In summary, the SePdx protein, specific to the green lineage, is a pyridoxine dehydrogenase with a potential dual function. It catalyzes the oxidation of PN in VitB6 biosynthesis and is also associated with the thylakoid membrane, connecting the PBS and PSI. These associations, combined with the physiological properties of the mutant strain, suggested that SePdx may play a role in the assembly of photosynthesis complexes. Hence, SePdx most likely links VitB6 biosynthesis and photosynthetic performance. Further research is required to determine whether SePdx performs both functions simultaneously or switches between them under specific conditions.

MATERIALS AND METHODS

Bioinformatics analysis

Homologous proteins of *SePdx* were identified through blast searches in the NCBI and UniProtKB databases (Pruitt et al., 2007; UniProt Consortium, 2019). The criteria for assessing protein homology included an *e*-value ≤ 0.05 and an identity $\geq 30\%$. For phylogenetic analyses, the Clustal W multiple alignment program

was used to align SePdx-like sequences from various representative species. A neighbor-joining phylogenetic tree was then constructed using MEGA11 with the Jones-Taylor-Thornton (JTT) model and 1000 bootstrap replicates. The resulting tree was visualized using the tool of Interactive Tree of Life (iTOL 6.7.5, 11) (Letunic & Bork, 2021). The evolutionary analysis was conducted using the BEAST v1.10.4 package (Drummond et al., 2012). A relaxed, uncorrelated molecular clock was used as the molecular clock model. Information about species divergence over time was sourced from the TimeTree website (<https://timetree.org/home>). Each Markov Chain Monte Carlo (MCMC) analysis was run for at least 50 million generations, with samples taken every 1000 generations. Convergence of chains and effective sample size (ESS) exceeding 200 were assessed using the tool Tracer (<http://tree.bio.ed.ac.uk/software/tracer/onquist>). The Tree Annotator program was utilized to summarize the trees into a maximum clade credibility (MCC) tree after eliminating the initial 10% as burn-in.

The prediction of signal peptides and transmembrane domains was performed using SignalP 6.0 (<https://services.healthtech.dtu.dk/services/SignalP-6.0/>) (Teufel et al., 2022) and PRED-TER (<http://athina.biol.uoa.gr/PRED-TER/>) (Viklund et al., 2008), respectively. Subcellular localization of proteins was predicted using CELLO (<http://cello.life.nctu.edu.tw/>) (Yu et al., 2006). The protein domain architecture of SePdx was characterized using the NCBI (CDD) database (<https://www.ncbi.nlm.nih.gov/cdd/>). The structural model of SePdx was generated using AlphaFold2 (<https://colab.research.google.com/github/sokrypton/ColabFold/blob/main/AlphaFold2.ipynb>) (Mirdita et al., 2022) and DeepMSA2 (<https://seq2fun.dcmf.med.umich.edu/DMFold>) (Zheng et al., 2024).

Construction and validation of *sepxd* deletion and complementation mutants

The *sepxd* knockout mutants were generated by natural transformation and double homologous recombination techniques. Homologous fragments of an 864-bp upstream sequence and an 881-bp downstream sequence flanking the *sepxd* gene were cloned into a suicide plasmid containing the *codA* gene. This plasmid was then introduced into *E. coli* DH5 α and naturally transformed into *Synechococcus* (Lea-Smith et al., 2016). Mutants were selected on BG-11 agar plates with 25 $\mu\text{g ml}^{-1}$ kanamycin. In order to achieve thorough segregation of the mutant, the selected mutants were streaked onto agar plates supplemented with 100 $\mu\text{g ml}^{-1}$ kanamycin. Positive clones were confirmed by PCR and sequencing (Figure S2). PCR was also used to verify that the *sepxd* gene knockout did not impact neighboring genes (Figure S2).

To generate a *sepxd*-complemented strain, the *sepxd* gene was amplified from the WT *Synechococcus* genome. The amplified gene was subsequently inserted into the pSyn_6 vector. The pSyn_6 vector is equipped with neutral site 1 (NS1) homologous recombination sites and a robust constitutive promoter derived from the *psbA* gene, which facilitates the high-level expression of *sepxd*. The resultant plasmid was then introduced into the *sepxd* knockout mutant strain through the natural transformation process. To determine the strains that were successfully complemented, a selection process was carried out on BG-11 agar plates supplemented with 50 $\mu\text{g ml}^{-1}$ of spectinomycin. The plates were then incubated at 30°C while being exposed to a continuous light intensity of 40 $\mu\text{mol photons m}^{-2} \text{sec}^{-1}$. Subsequently, PCR analysis was conducted to verify the presence of the *sepxd* gene in the complemented strains.

A complete list of primers used in these experiments is available in Dataset S5.

LC-MS analysis of PL and PN

For qualitative and quantitative content analyses of PL and PN, WT and $\Delta sepx$ mutant cells were cultured in BG-11 media until they reached an optical density (OD) of approximately 1.0 at 730 nm. Subsequently, the cultures were harvested, and 400 μ l of petroleum ether was added for lipid removal through sonication for 30 min. The petroleum ether was then discarded, and 400 μ l of a 1% phosphoric acid aqueous solution was added to the residue for VitB6 extraction. The LC-MS analysis was conducted using a Hybrid Quadrupole-TOF LC-MS/MS Mass Spectrometer coupled to a Shimadzu LC-30AD chromatography system (LC-30AD, Shimadzu, Kyoto, Japan). Standard PL and PN were procured from Shanghai Yuanye Biotechnology Co., Ltd.

Enzyme assays

The *sepx* gene was cloned into the pMBP_C vector and transformed into the *E. coli* Rosetta 2(DE3) strain for heterologous expression. Pyridoxine dehydrogenase activity was measured according to the previously described method with some modifications (Huang et al., 2014). Each reaction mixture (1.0 ml) contained 0.2 mM PN, 0.2 mM NADP⁺, 50 mM citrate buffer (pH 6.5), and 500 μ g of total protein. The negative control was protein extracts from *E. coli* expressing the pMBP_C empty vector. The reaction was performed at 37°C for 30 min and was terminated by the addition of 0.3 ml of 3 M HClO₄. The mixture was then centrifuged at 12 840 g for 15 min at 4°C to remove any precipitate. To the supernatant, 1 ml of distilled water and 0.2 ml of phenylhydrazine (0.1 M) were added, followed by incubation at 60°C for 20 min. The formation of PL was detected by measuring the absorbance at 410 nm.

Growth curve and stress treatment

Synechococcus cells were cultured in BG-11 liquid media under 40 μ mol photons m⁻² sec⁻¹. The cells were then washed three times by centrifugation (1000 g, 20 min, room temperature) and resuspended in BG-11 media to obtain an initial optical density of 0.025 at 730 nm. Experiments were conducted in triplicate with 50-ml culture volumes. OD730 nm values were measured daily for 11 days. Photographs of the algal cultures were taken at specific OD730 nm values of 0.5 and 1.0 to document the growth stages visually.

According to Kim et al. (2017), oxidative stress induced by H₂O₂ was observed in BG-11 media with an initial OD730 nm of 0.5. The strains were exposed to 20 mM H₂O₂, and OD730 nm was measured daily until the end of the experiment. Salt stress was stimulated by culturing the strains in BG-11 medium supplemented with 0.3 mM NaCl at 30°C under continuous light with shaking. Photographs were taken to document the appearance of the algal liquid. For growth tests on a solid medium, exponentially growing cells were serially diluted in water and deposited as drops onto BG-11 agarose plates. The plates were then incubated under high light conditions (HL) at an intensity of 150 μ mol photons m⁻² sec⁻¹ to assess growth under these specific light conditions. In the nitrogen limitation experiments, BG-11 agarose plates without nitrogen sources were used and cultured under continuous light.

Subcellular localization

To investigate the subcellular localization of SePdx in *Synechococcus*, the strategy employed in this study involved cloning the ORF genes into a backbone plasmid harboring the mNeonGreen (mNG) coding gene, 3 × FLAG coding gene, kanamycin resistance gene, and *codA* negative selection markers (Figure S7). The use of

mNG was aimed to enhance the brightness and photostability of the fusion protein when expressed *in vivo*. Subsequently, the recombinant plasmid was introduced into *Synechococcus* cells via transformation. The marker mutants with tagged markers and antibiotic cassettes were initially chosen on BG-11 agar supplemented with 200 μ g ml⁻¹ kanamycin and subsequently selected on 0.1 g L⁻¹ 5-fluorocytosine to obtain the mutant without the antibiotic cassette. To ensure the purity of the tagged mutant, colony PCR was performed. The mutant cells were visualized using a two-photon confocal microscope (Leica TCS SP8 MP, Leica Microsystems, Wetzlar, Germany), with fluorescent signals detected at an excitation wavelength of 488 nm and an emission range of 520–600 nm. Furthermore, to detect the autofluorescent signal of chlorophyll, an excitation wavelength of 561 nm and an emission range of 660–700 nm was utilized. Image analysis was performed using ImageJ software.

Hoechst33342 and PI staining assays

The phenotypic characteristics of cell death were assessed using a Hoechst33342/PI double staining assay. The cultures were grown in BG-11 media until they reached an optical density of 1.0 at 730 nm. The culture broth (1 ml) was centrifuged at 4°C and 4000 rpm for 15 min and then incubated with 100 μ l of staining solution (10 μ M PI and 10 μ g ml⁻¹ Hoechst33342 in PBS) for 20 min at room temperature. The cells were then washed twice with PBS. Stained images were captured using a two-photon laser scanning confocal microscope (Leica TCS SP8 MP, Leica Microsystems, Wetzlar, Germany). Hoechst 33342 has a maximum excitation wavelength of 346 nm and a maximum emission wavelength of 460 nm, while the excitation and emission wavelengths of the PI-DNA complex are 535 and 615 nm, respectively.

Transmission electron microscopy (TEM)

The morphology of the *Synechococcus* cells was analyzed by TEM. The cells were cultured to an optical density of 1.0 at 730 nm. Harvested cells were fixed in a solution containing 2.5% glutaraldehyde for electron fixation, followed by post-fixation in 1% osmic acid. Dehydration was performed using a graded series of ethanol (50–100%). Subsequently, the specimens were embedded and sliced into 70 nm thick sections. Ultrathin sections were stained with a 2% uranyl acetate solution and a lead stain solution (Sigma) and heated for 10 min under infrared light. The specimen sections were further stained with uranyl acetate and alkaline lead citrate. The images were taken using a Hitachi HT-7800 TEM instrument (Hitachi, Ltd., Tokyo, Japan) at an accelerating voltage of 80 kV.

Transcriptome sequencing and data processing

To investigate gene expression levels, WT and $\Delta sepx$ mutant cells were cultured to an optical density of 1.0 at 730 nm. The harvested cells were frozen and sent to Personalbio Co., Ltd. (Shanghai, China) for RNA extraction, library preparation, mapping, and bioinformatics analysis. The prepared libraries were sequenced on an Illumina Hi-Seq platform using the 2 × 150 bp paired-end sequencing strategy. To process the obtained sequencing data, clean reads were aligned to the *Synechococcus* genome using TopHat v2.0.12. The HTSeq 0.6.1p2 tool was employed to determine the read counts mapped to each gene. Subsequently, Fragments Per Kilobase of transcript per Million mapped reads (FPKM) values were computed for individual genes. The FPKM values were calculated based on the gene length and the mapped read counts. Genes were categorized as either expressed (FPKM ≥ 1) or unexpressed (FPKM < 1). The DESeq (v1.38.3) package was used

to analyze differential gene expression, with a significance threshold level of q value <0.05 and an absolute $\log_2\text{FoldChange}$ > 1 .

Proteomic analysis

Cells were lysed with a lysis buffer to extract the proteome, followed by the addition of pre-chilled acetone. The mixture was then incubated at -20°C overnight to induce protein precipitation. Subsequently, the acetone was removed, and the samples were washed, reconstituted in lysis buffer, and subjected to centrifugation to isolate membrane proteins. The protein solution was quantified, enzymatically digested, and purified with C18 solid-phase extraction columns. Subsequently, the samples underwent separation and analysis through liquid chromatography–tandem mass spectrometry (LC-MS/MS, Thermo Fisher Scientific, Shanghai, China). The mass spectrometry data were processed in a data-independent acquisition (DIA) mode and compared against the species-specific protein database for qualitative analysis. The mass spectrometry data were analyzed using Spectronaut software (version 17.2) with specific search parameters: selection of the species-specific protein database, trypsin digestion allowing up to two missed cleavage sites, 10 ppm precursor ion mass tolerance, 0.02 Da fragment ion mass tolerance, Carbamidomethyl (C) as a fixed modification, Oxidation (M) and Acetyl (N-terminal) as variable modifications, control of false discovery rate (FDR) for peptides and proteins at $<1.0\%$, and each protein identification required at least one unique peptide.

PBS-thylakoid membrane isolation and immunoblot analysis

PBS-thylakoid membranes were prepared following a previously described procedure with slight modifications (Zhao et al., 2020). *Synechococcus* cells were pelleted by centrifugation, washed with buffer PC (0.5 M potassium phosphate, 0.3 M sodium citrate), and resuspended in buffer SPC (0.5 M sucrose, 0.5 M potassium phosphate, 0.3 M sodium citrate). Cell pellets were disrupted using glass beads (diameter = 212–300 μm) by vortexing for six cycles (1 min vortexing followed by 30 sec in an ice bath) and subsequent centrifugation. The crude extract was centrifuged at 3000 g for 5 min to remove the glass beads and unbroken cells. Crude PBS-thylakoid membranes were centrifuged at 18 000 g for 30 min and resuspended in SPC buffer. To isolate pure PBS-thylakoid membranes, a step sucrose gradient (2.0, 1.3, 1.0, and 0.75 M) was utilized, followed by centrifugation at 36 000 rpm in a Beckman RPS40 rotor for 1 h at 4°C . Samples from the 0.75–1.0 M and 1.0–1.3 M sucrose interfaces were collected for 12.5% (w/v) SDS-PAGE and immunoblotting. The proteins were probed with a 1:1000 dilution of anti-Flag Monoclonal antibody, followed by a 1:5000 dilution of anti-Flag secondary antibody.

Blue native (BN)-PAGE

For denatured electrophoresis, crude extracts of the thylakoid membrane were denatured as previously described (Ma et al., 2017). Proteins were then separated by 12.5% (w/v) SDS-PAGE, and transferred to a PVDF membrane (Beyotime) (Huokko et al., 2021). The isolated membranes were washed with a washing buffer containing 330 mM sorbitol, 50 mM Bis-Tris (pH 7.0), and 250 $\mu\text{g ml}^{-1}$ of Pefabloc (Sigma). They were then suspended in a solution of 20% glycerol (w/v), 25 mM Bis-Tris (pH 7.0), 10 mM MgCl_2 , and 0.01 unit ml^{-1} RNase-Free DNase RQ1 (Promega), resulting in a final protein concentration of 20 $\mu\text{g } \mu\text{l}^{-1}$. After 10 min of incubation on ice, 3% *n*-dodecyl- β -D-maltoside was added in an equal volume. The samples were solubilized on ice for 10 min, then at room temperature for 20 min, followed by centrifugation

at 18 000 g for 15 min to remove the insoluble material. The resulting supernatant was collected and mixed with 1/10 volume of 0.1 M EDTA and 1/10 volume of sample buffer containing 5% Serva blue G, 200 mM Bis-Tris (pH 7.0), 75% sucrose, and 1 M ϵ -amino-*n*-caproic acid. Subsequently, the samples were loaded onto Native-PAGE Bis-Tris protein gels with a 4–16% gradient (Real-Times). The voltage was gradually increased from 50 to 200 V during the gel run. Finally, the samples were observed by staining with Coomassie Brilliant Blue.

Pigment content and photosynthetic oxygen evolution

To determine the chlorophyll content, cells of WT, *sepx* deletion, and complemented strains (1.0 ml, OD730 nm = 1.0) were collected and centrifuged. The pellet was washed twice, and the pigments were extracted by adding 1.0 ml of methyl alcohol. The chlorophyll content was measured using a spectrophotometer (UV-5500; Shanghai Metash Instruments Co., Ltd.) according to the formula: Chlorophyll (chl) a ($\mu\text{g ml}^{-1}$) = $A_{665\text{ nm}} \times 13.9$ (Arnon, 1949). Phycocyanin and carotenoid pigments were quantified using *in vivo* absorption measurements, as described by Kouchkovsky and Sigalat (1975) and Mantovani et al. (2022).

The oxygen consumption rate was measured in 2.0 ml of cells (OD730 nm = 1.0) suspended in 10 mM NaHCO_3 at 30°C . An oxyLab oxygen electrode (Hanshatech) was used for the measurements. Simultaneously, Chl fluorescence was recorded along with oxygen evolution rates. The oxygen evolution rates were adjusted based on the Chl *a* fluorescence values for each experimental replicate.

Absorption and fluorescence spectroscopy

Full-length absorption spectra of cells were measured at room temperature using SpectraMax M Series Microplate Reader M5 (Molecular Devices, CA, USA) and normalized to absorption values at 730 nm (Pascual-Aznar et al., 2021). Room temperature fluorescence emission spectra were measured with an excitation wavelength of 545 nm and an emission wavelength of 600–750 nm by a fluorescence spectrofluorometer (SpectraMax; Molecular Devices, CA, USA) (Zhao et al., 2016).

Phycobilisome (PBS) isolation

In accordance with the method described by Zavřel et al. (2018), WT and mutant strains were collected at an optical density of 1.0 at 730 nm, followed by centrifugation. The phycobiliproteins in the pellet were extracted using 1 ml of PBS. The absorbance of phycocyanobilins in phycocyanin and allophycocyanin was measured against a PBS buffer blank containing 154 mM NaCl, 5.599 mM Na_2HPO_4 , and 1.058 mM KH_2PO_4 at 615 (A615) and 652 nm (A652), respectively, while the absorbance of cellular debris was measured at 720 nm (A720). The concentrations of phycocyanin and allophycocyanin were calculated using the Equations (1) and (2) proposed by Bennett and Bogorad (1973):

$$\text{Phycocyanin} = ((A_{615} - A_{720}) - 0.474 \times (A_{652} - A_{720})) / 5.34 / 25 \text{ [mg ml}^{-1}\text{]} \quad (1)$$

$$\text{Allophycocyanin} = ((A_{652} - A_{720}) - 0.208 \times (A_{615} - A_{720})) / 5.09 / 25 \text{ [mg ml}^{-1}\text{]} \quad (2)$$

Subsequently, the proteins were separated using 12.5% (w/v) SDS-PAGE. The substrate was visualized either by Coomassie brilliant blue staining (0.25% Coomassie brilliant blue R250, 45%

methanol, and 10% acetic acid) or zinc sulfate staining (100 mM ZnSO₄) (Raps, 1990).

Affinity purification and mass spectrometry (AP-MS)

To investigate protein–protein interactions involving SePdx, a combination of affinity purification (AP) and mass spectrometry (MS) was employed. To facilitate purification, a FLAG tag sequence was inserted at the 3' end of the *sepx* gene. Cultures were grown in 200 ml of BG-11 media under controlled conditions (OD₇₃₀ of 1.0, 30°C, and 40 μmol photons m⁻² sec⁻¹). The cells were then resuspended in 500 μl of pre-chilled IP buffer (100 mM HEPES, 100 mM KOAc, 4 mM Mg (OAc)₂ · 4H₂O, 400 mM sorbitol, pH 6.8) containing 2% digitonin and incubated on ice for 30 min. Cell lysis was achieved by vortexing with glass beads. Subsequently, the lysates underwent affinity purification using anti-FLAG M2-bound Dynabeads (Invitrogen). After purification, proteins bound to anti-FLAG M2 beads were eluted using 50 μg ml⁻¹ FLAG peptide (Sigma) and analyzed by MS.

For MS analysis, proteins were subjected to acetone precipitation, reduction, alkylation, trypsin digestion, and desalting according to established protocols (Wong et al., 2006). The resulting peptides were reconstituted in 10 μl of 0.1% formic acid (FA) and separated by online nanoscale reversed-phase capillary liquid chromatography (Easy-nLC 1000; Thermo Fisher Scientific, Shanghai, China). Separation was performed at low pH using a C18 reversed-phase column (150 μm × 250 mm, 1.9 μm). The peptides were then analyzed using a Thermo Q Exactive HF-X hybrid quadrupole Orbitrap mass spectrometer (Thermo Fisher Scientific, Shanghai, China). The MS parameters were set as follows: measurement scan in the mass range 380–1650 m/z, scan time 60 min, blocking mass activated, and 200 m/z resolution of 120 000. The automatic gain control (AGC) target value was set to 3e6, with a maximum injection time of 80 msec. The normalized collision energy was set at 30%. The secondary scan resolution was 15 000, the AGC was set to 2e4, and the maximum injection time was 19 msec. Precursor ions were filtered based on their charge state (including +2 to +8 charges) and dynamically excluded for 15 sec to avoid repeated analysis of the same ions.

Bacterial two-hybrid (B2H) assays

To investigate protein interactions, bacterial two-hybrid (B2H) assays were performed using the bacterial adenylate cyclase two-hybrid system kit (BACTH System kit; Euromedex), as described by Karimova et al. (1998). The *sepx* and relevant genes of interest were cloned into the pKT25 and pUT18C plasmids, respectively, using the primers listed in Dataset S5. The constructed plasmids containing the bait and prey genes were co-transformed into *E. coli* BTH101 cells. The transformed colonies were cultured overnight at 30°C in LB media supplemented with appropriate selection (100 μg ml⁻¹ ampicillin and 50 μg ml⁻¹ kanamycin). Subsequently, 2 μl of each culture was plated on MacConkey agar plates with the appropriate selection and 500 μM isopropyl-beta-D-1-thiogalactopyranoside (IPTG). The plates were then incubated at 30°C for 2–4 days. The interaction between the two fusion proteins was assessed based on the appearance of lac-inducing colonies, which appeared red on MacConkey agar. In contrast, the absence of induction, as indicated by white colonies, suggested no interaction between the fusion proteins.

The quantification of functional complementation caused by protein–protein interactions was determined by measuring β-galactosidase activity in liquid cultures. For this purpose, permeabilized cells having an optical density of 1.0 at 600 nm were used with o-nitrophenol-β-galactoside (ONPG) as the substrate. In

summary, the lysed cells were quantified for protein concentration and diluted to 500 μg ml⁻¹. Then, 200 μl of the diluted lysate sample was mixed with 450 μl of a 20 mM ONPG solution (20 mM phosphate buffer, pH 7.0). The mixture was incubated at 37°C for 20 min, and the reaction was stopped by adding 500 μl of 0.1 M sodium carbonate. The released o-nitrophenol (ONP) was then measured at 420 nm.

Protein docking

The X-ray crystal structures of CpcA1 (PDB ID 4H0M), CpcB1 (PDB ID 4H0M), and PsaE (PDB ID 6KIG) were obtained from the Protein Data Bank (<http://www.rcsb.org/>). The predicted structure of SePdx was generated using AlphaFold, as described above. Initial protein docking was performed using the ClusPro 2.0 algorithm (<https://cluspro.org>) (Desta et al., 2020). Flexible docking was then performed with RosettaDock (versions accessible at <http://www.rosettacommons.org>) (Chaudhury et al., 2011) based on the rigid docking results. The final results were selected using Rosetta's built-in score module. Interactions between proteins were analyzed using the "LIGPLOT" module of the LigPlot+ program (<https://www.ebi.ac.uk/thornton-srv/software/LIGPLOT/>) (Laskowski & Swindells, 2011). Additionally, the overall interaction binding energy and the binding energy between key amino acids were assessed using the Interface_analyzer and Interface_energy modules of Rosetta, respectively. The structural models were visually evaluated using PyMol 2.2.0.

Site-directed mutagenesis

Site-directed mutagenesis was performed to introduce amino acid substitutions (T5A, D28A, T31R, R96A, Y144A, R189A, Q214A, and G299A) into the pKT25-SePdx plasmid using the Fast Site-Directed Mutagenesis Kit (Tiangen). The introduced amino acid substitutions were verified by full-length gene sequencing. Subsequently, the mutated plasmids were co-transformed into *E. coli* BTH101 cells along with PKT18C-CpcA1 or PKT18C-PsaE plasmid. The B2H assays and β-galactosidase activities were carried out as described above.

AUTHOR CONTRIBUTIONS

SF, WL, ZC: Investigation, methodology, software, data curation. ZW, XC, SZ, MD, JY: Investigation, data curation. LC: Conceptualization, writing review and editing, funding acquisition. GZ: Conceptualization, investigation, writing original draft, writing review and editing, funding acquisition.

ACKNOWLEDGMENTS

We would like to express our gratitude to Prof. Luke C. M. Mackinder from the University of York for his assistance with the AP-MS data analysis and valuable suggestions. We also acknowledge the BiotechPack company for conducting the LC-MS analyses of PL and PN. Additionally, we appreciate Figdraw for their contributions in modifying the hypothetical functional model. This study was funded by the National Natural Science Foundation of China (Grant No. 31970367; 31640002), the Natural Science Foundation of Shandong Province (Grant No. ZR2024MC202), the Qingchuang Talents Induction Program of Shandong Higher Education Institution in 2021, and the Taishan Scholar Program of Shandong Province (tsqn201909168).

CONFLICT OF INTEREST

The authors declare no competing interests.

DATA AVAILABILITY STATEMENT

All relevant data can be found within the manuscript and its supporting materials. The raw transcriptomic analysis dataset, proteomic dataset, and mass spectrometry dataset are all included in the supporting datasets.

SUPPORTING INFORMATION

Additional Supporting Information may be found in the online version of this article.

Figure S1. Schematic model depicting the DXP-dependent, DXP-independent, and salvage pathways of vitamin B6 biosynthesis in *Synechococcus*.

Figure S2. Generation of $\Delta sepx$ knockout mutant and LC/MS analysis.

Figure S3. Evolutionary relationships of SePdx and its homolog proteins.

Figure S4. Bioinformation of SePdx protein.

Figure S5. Cell morphology of *Synechococcus* cells.

Figure S6. The effects of *sepx* gene knockout on the transcriptome and proteome of *Synechococcus*.

Figure S7. Generation of *Synechococcus* tagging mutant.

Figure S8. Purification of PBS-thylakoid membranes (TM) by density gradient centrifugation and the detection of phycobilisome.

Dataset S1. SePdx and homologous protein sequences.

Dataset S2. Transcriptomic analysis data.

Dataset S3. Proteomic data.

Dataset S4. Affinity purification and mass spectrometry (AP-MS) data.

Dataset S5. List of primer sequences.

REFERENCES

- Adir, N. (2005) Elucidation of the molecular structures of components of the phycobilisome: reconstructing a giant. *Photosynthesis Research*, **85**, 15–32.
- Arnon, D.I. (1949) Copper enzymes in isolated chloroplasts. Polyphenoloxidase in *Beta vulgaris*. *Plant Physiology*, **24**, 1–15.
- Bennett, A. & Bogorad, L. (1973) Complementary chromatic adaptation in a filamentous blue-green alga. *The Journal of Cell Biology*, **58**, 419–435.
- Black, C.C. & Pietro, A.S. (1968) Vitamin B6 activity in photosynthetic reactions. *Archives of Biochemistry and Biophysics*, **128**, 482–487.
- Cao, P., Cao, D., Si, L., Su, X., Tian, L., Chang, W. *et al.* (2020) Structural basis for energy and electron transfer of the photosystem I-IsiA-flavodoxin supercomplex. *Nature Plants*, **6**, 167–176.
- Chaudhury, S., Berrondo, M., Weitzner, B.D., Muthu, P., Bergman, H. & Gray, J.J. (2011) Benchmarking and analysis of protein docking performance in Rosetta v3.2. *PLoS One*, **6**, e22477.
- Colinas, M., Eisenhut, M., Tohge, T., Pesquera, M., Fernie, A.R., Weber, A.P. *et al.* (2016) Balancing of B6 vitamers is essential for plant development and metabolism in Arabidopsis. *Plant Cell*, **28**, 439–453.
- Desta, I.T., Porter, K.A., Xia, B., Kozakov, D. & Vajda, S. (2020) Performance and its limits in rigid body protein-protein docking. *Structure*, **28**, 1071–1081.e1073.
- di Salvo, M.L., Contestabile, R. & Safo, M.K. (2011) Vitamin B(6) salvage enzymes: mechanism, structure and regulation. *Biochimica et Biophysica Acta*, **1814**, 1597–1608.
- Drummond, A.J., Suchard, M.A., Xie, D. & Rambaut, A. (2012) Bayesian phylogenetics with BEAUti and the BEAST 1.7. *Molecular Biology and Evolution*, **29**, 1969–1973.
- Elanskaya, I.V., Zlenko, D.V., Lukashev, E.P., Suzina, N.E., Kononova, I.A. & Stadnichuk, I.N. (2018) Phycobilisomes from the mutant cyanobacterium *Synechocystis* sp. PCC 6803 missing chromophore domain of ApcE. *Biochimica et Biophysica Acta - Bioenergetics*, **1859**, 280–291.
- Havaux, M., Guedeney, G., Hagemann, M., Yermenko, N., Matthijs, H.C. & Jeanjean, R. (2005) The chlorophyll-binding protein IsiA is inducible by high light and protects the cyanobacterium *Synechocystis* PCC6803 from photooxidative stress. *FEBS Letters*, **579**, 2289–2293.
- Havaux, M., Ksas, B., Szewczyk, A., Rumeau, D., Franck, F., Caffarri, S. *et al.* (2009) Vitamin B6 deficient plants display increased sensitivity to high light and photo-oxidative stress. *BMC Plant Biology*, **9**, 130.
- Heinrich, M.L. & Grossman, A.R. (2013) The GreenCut: re-evaluation of physiological role of previously studied proteins and potential novel protein functions. *Photosynthesis Research*, **116**, 427–436.
- Herrero, S., González, E., Gillikin, J.W., Véléz, H. & Daub, M.E. (2011) Identification and characterization of a pyridoxal reductase involved in the vitamin B6 salvage pathway in Arabidopsis. *Plant Molecular Biology*, **76**, 157–169.
- Hu, P.P., Hou, J.Y., Xu, Y.L., Niu, N.N., Zhao, C., Lu, L. *et al.* (2020) The role of lyases, NblA and NblB proteins and bilin chromophore transfer in restructuring the cyanobacterial light-harvesting complex. *The Plant Journal*, **102**, 529–540.
- Huang, S., Zhang, J., Tao, Z., Lei, L., Yu, Y. & Huang, L. (2014) Enzymatic conversion from pyridoxal to pyridoxine caused by microorganisms within tobacco phyllosphere. *Plant Physiology and Biochemistry*, **85**, 9–13.
- Huokko, T., Ni, T., Dykes, G.F., Simpson, D.M., Brownridge, P., Conradi, F.D. *et al.* (2021) Probing the biogenesis pathway and dynamics of thylakoid membranes. *Nature Communications*, **12**, 3475.
- Ito, T. & Downs, D.M. (2020) Pyridoxal reductase, PdxL, is critical for salvage of pyridoxal in *Escherichia coli*. *Journal of Bacteriology*, **202**, e00056-20.
- Karimova, G., Pidoux, J., Ullmann, A. & Ladant, D. (1998) A bacterial two-hybrid system based on a reconstituted signal transduction pathway. *Proceedings of the National Academy of Sciences of the United States of America*, **95**, 5752–5756.
- Karpowicz, S.J., Prochnik, S.E., Grossman, A.R. & Merchant, S.S. (2011) The GreenCut2 resource, a phylogenomically derived inventory of proteins specific to the plant lineage. *The Journal of Biological Chemistry*, **286**, 21427–21439.
- Kato, K., Nagao, R., Jiang, T.Y., Ueno, Y., Yokono, M., Chan, S.K. *et al.* (2019) Structure of a cyanobacterial photosystem I tetramer revealed by cryo-electron microscopy. *Nature Communications*, **10**, 4929.
- Kim, Y.S., Kim, I.S., Boyd, J.S., Taton, A., Golden, J.W. & Yoon, H.S. (2017) Enhanced biomass and oxidative stress tolerance of *Synechococcus elongatus* PCC 7942 overexpressing the DHAR gene from *Brassica juncea*. *Biotechnology Letters*, **39**, 1499–1507.
- Kondo, K., Geng, X.X., Katayama, M. & Ikeuchi, M. (2005) Distinct roles of CpcG1 and CpcG2 in phycobilisome assembly in the cyanobacterium *Synechocystis* sp. PCC 6803. *Photosynthesis Research*, **84**, 269–273.
- Kondo, K., Mullineaux, C.W. & Ikeuchi, M. (2009) Distinct roles of CpcG1-phycobilisome and CpcG2-phycobilisome in state transitions in a cyanobacterium *Synechocystis* sp. PCC 6803. *Photosynthesis Research*, **99**, 217–225.
- Kondo, K., Ochiai, Y., Katayama, M. & Ikeuchi, M. (2007) The membrane-associated CpcG2-phycobilisome in *Synechocystis*: a new photosystem I antenna. *Plant Physiology*, **144**, 1200–1210.
- Kouchkovsky, Y. & Sigalat, C. (1975) Fractionnement et caractérisation de l'appareil photosynthétique de l'algue bleue unicellulaire *Anacystis nidulans*. *Physiologie Végétale*, **13**, 243–258.
- Krauspe, V., Fahrner, M., Spät, P., Steglich, C., Frankenberg-Dinkel, N., Maček, B. *et al.* (2021) Discovery of a small protein factor involved in the coordinated degradation of phycobilisomes in cyanobacteria. *Proceedings of the National Academy of Sciences of the United States of America*, **118**, e201227118.
- Labella, J.L., Cantos, R., Espinosa, J., Forcada-Nadal, A., Rubio, V. & Contreras, A. (2017) PipY, a member of the conserved COG0325 family of PLP-binding proteins, expands the cyanobacterial nitrogen regulatory network. *Frontiers in Microbiology*, **8**, 1244.
- Laskowski, R.A. & Swindells, M.B. (2011) LigPlot+: multiple ligand-protein interaction diagrams for drug discovery. *Journal of Chemical Information and Modeling*, **51**, 2778–2786.
- Lea-Smith, D.J., Vasudevan, R. & Howe, C.J. (2016) Generation of marked and markerless mutants in model cyanobacterial species. *Journal of Visualized Experiments*, **111**, 54001.
- Letunic, I. & Bork, P. (2021) Interactive tree of life (iTOL) v5: an online tool for phylogenetic tree display and annotation. *Nucleic Acids Research*, **49**, W293–w296.

- Liu, H., Weisz, D.A., Zhang, M.M., Cheng, M., Zhang, B., Zhang, H. *et al.* (2019) Phycobilisomes harbor FNR(L) in cyanobacteria. *mBio*, **10**, e00669-19.
- Ma, F., Zhang, X., Zhu, X., Li, T., Zhan, J., Chen, H. *et al.* (2017) Dynamic changes of IsiA-containing complexes during long-term iron deficiency in *Synechocystis* sp. PCC 6803. *Molecular Plant*, **10**, 143–154.
- Mackinder, L.C.M., Chen, C., Leib, R.D., Patena, W., Blum, S.R., Rodman, M. *et al.* (2017) A spatial interactome reveals the protein organization of the algal CO(2)-concentrating mechanism. *Cell*, **171**, 133–147.e114.
- Mangel, N., Fudge, J.B., Li, K.T., Wu, T.Y., Tohge, T., Fernie, A.R. *et al.* (2019) Enhancement of vitamin B(6) levels in rice expressing *Arabidopsis* vitamin B(6) biosynthesis *de novo* genes. *The Plant Journal*, **99**, 1047–1065.
- Mantovani, O., Reimann, V., Haffner, M., Hermann, F.P., Selim, K.A., Forchhammer, K. *et al.* (2022) The impact of the cyanobacterial carbon-regulator protein SbtB and of the second messengers cAMP and c-di-AMP on CO₂-dependent gene expression. *The New Phytologist*, **234**, 1801–1816.
- Marx, A. & Adir, N. (2013) Allophycocyanin and phycocyanin crystal structures reveal facets of phycobilisome assembly. *Biochimica et Biophysica Acta*, **1827**, 311–318.
- Mills, L.A., McCormick, A.J. & Lea-Smith, D.J. (2020) Current knowledge and recent advances in understanding metabolism of the model cyanobacterium *Synechocystis* sp. PCC 6803. *Bioscience Reports*, **40**, BSR20193325.
- Mirdita, M., Schütze, K., Moriwaki, Y., Heo, L., Ovchinnikov, S. & Steinegger, M. (2022) ColabFold: making protein folding accessible to all. *Nature Methods*, **19**, 679–682.
- Morita, T., Takegawa, K. & Yagi, T. (2004) Disruption of the *plr1+* gene encoding pyridoxal reductase of *Schizosaccharomyces pombe*. *Journal of Biochemistry*, **135**, 225–230.
- Nield, J., Rizkallah, P.J., Barber, J. & Chayen, N.E. (2003) The 1.45 Å three-dimensional structure of C-phycocyanin from the thermophilic cyanobacterium *Synechococcus elongatus*. *Journal of Structural Biology*, **141**, 149–155.
- Pascual-Aznar, G., Konert, G., Bečkov, M., Kotabov, E., Gardian, Z., Knopov, J. *et al.* (2021) Psb35 protein stabilizes the CP47 assembly module and associated high-light inducible proteins during the biogenesis of photosystem II in the cyanobacterium *Synechocystis* sp. PCC6803. *Plant & Cell Physiology*, **62**, 178–190.
- Pruitt, K.D., Tatusova, T. & Maglott, D.R. (2007) NCBI reference sequences (RefSeq): a curated non-redundant sequence database of genomes, transcripts and proteins. *Nucleic Acids Research*, **35**, D61–D65.
- Raps, S. (1990) Differentiation between phycobiliprotein and colorless linker polypeptides by fluorescence in the presence of ZnSO₄. *Plant Physiology*, **92**, 358–362.
- Raschke, M., Boycheva, S., Crèvecoeur, M., Nunes-Nesi, A., Witt, S., Fernie, A.R. *et al.* (2011) Enhanced levels of vitamin B(6) increase aerial organ size and positively affect stress tolerance in *Arabidopsis*. *The Plant Journal*, **66**, 414–432.
- Richaud, C., Zabulon, G., Joder, A. & Thomas, J.C. (2001) Nitrogen or sulfur starvation differentially affects phycobilisome degradation and expression of the *nblA* gene in *Synechocystis* strain PCC 6803. *Journal of Bacteriology*, **183**, 2989–2994.
- Rubin, B.E., Wetmore, K.M., Price, M.N., Diamond, S., Shultzaberger, R.K., Lowe, L.C. *et al.* (2015) The essential gene set of a photosynthetic organism. *Proceedings of the National Academy of Sciences of the United States of America*, **112**, E6634–E6643.
- Rueschhoff, E.E., Gillikin, J.W., Sederoff, H.W. & Daub, M.E. (2013) The SOS4 pyridoxal kinase is required for maintenance of vitamin B6-mediated processes in chloroplasts. *Plant Physiology and Biochemistry*, **63**, 281–291.
- Sang, Y., Locy, R.D., Goertzen, L.R., Rashotte, A.M., Si, Y., Kang, K. *et al.* (2011) Expression, in vivo localization and phylogenetic analysis of a pyridoxine 5'-phosphate oxidase in *Arabidopsis thaliana*. *Plant Physiology and Biochemistry*, **49**, 88–95.
- Sato, T., Minagawa, S., Kojima, E., Okamoto, N. & Nakamoto, H. (2010) HtpG, the prokaryotic homologue of Hsp90, stabilizes a phycobilisome protein in the cyanobacterium *Synechococcus elongatus* PCC 7942. *Molecular Microbiology*, **76**, 576–589.
- Tambasco-Studart, M., Tews, I., Amrhein, N. & Fitzpatrick, T.B. (2007) Functional analysis of PDX2 from *Arabidopsis*, a glutaminase involved in vitamin B6 biosynthesis. *Plant Physiology*, **144**, 915–925.
- Tambasco-Studart, M., Titiz, O., Raschke, T., Forster, G., Amrhein, N. & Fitzpatrick, T.B. (2005) Vitamin B6 biosynthesis in higher plants. *Proceedings of the National Academy of Sciences of the United States of America*, **102**, 13687–13692.
- Teufel, F., Almagro Armenteros, J.J., Johansen, A.R., Gislason, M.H., Pihl, S.I., Tsirigos, K.D. *et al.* (2022) SignalP 6.0 predicts all five types of signal peptides using protein language models. *Nature Biotechnology*, **40**, 1023–1025.
- Ungerer, J., Lin, P.C., Chen, H.Y. & Pakrasi, H.B. (2018) Adjustments to photosystem stoichiometry and electron transfer proteins are key to the remarkably fast growth of the cyanobacterium *Synechococcus elongatus* UTEX 2973. *mBio*, **9**, e02327-17.
- UniProt Consortium. (2019) UniProt: a worldwide hub of protein knowledge. *Nucleic Acids Research*, **47**, D506–d515.
- Vanderschuren, H., Boycheva, S., Li, K.T., Szydlowski, N., Grisse, W. & Fitzpatrick, T.B. (2013) Strategies for vitamin B6 biofortification of plants: a dual role as a micronutrient and a stress protectant. *Frontiers in Plant Science*, **4**, 143.
- Viklund, H., Bernsel, A., Skwark, M. & Elofsson, A. (2008) SPOCTOPUS: a combined predictor of signal peptides and membrane protein topology. *Bioinformatics*, **24**, 2928–2929.
- Wang, J., Huang, X., Ge, H., Wang, Y., Chen, W., Zheng, L. *et al.* (2022) The quantitative proteome atlas of a model cyanobacterium. *Journal of Genetics and Genomics*, **49**, 96–108.
- Watanabe, M. & Ikeuchi, M. (2013) Phycobilisome: architecture of a light-harvesting supercomplex. *Photosynthesis Research*, **116**, 265–276.
- Watanabe, M., Semchonok, D.A., Webber-Birungi, M.T., Ehira, S., Kondo, K., Narikawa, R. *et al.* (2014) Attachment of phycobilisomes in an antenna-photosystem I supercomplex of cyanobacteria. *Proceedings of the National Academy of Sciences of the United States of America*, **111**, 2512–2517.
- Wong, J.J., Pung, Y.F., Sze, N.S. & Chin, K.C. (2006) HERC5 is an IFN-induced HECT-type E3 protein ligase that mediates type I IFN-induced ISGylation of protein targets. *Proceedings of the National Academy of Sciences of the United States of America*, **103**, 10735–10740.
- Yadav, S., Centola, M., Glaesmann, M., Pogoryelov, D., Ladig, R., Heilemann, M. *et al.* (2022) Cyclophilin *anaCyp40* regulates photosystem assembly and phycobilisome association in a cyanobacterium. *Nature Communications*, **13**, 1690.
- Yu, C.S., Chen, Y.C., Lu, C.H. & Hwang, J.K. (2006) Prediction of protein subcellular localization. *Proteins*, **64**, 643–651.
- Yu, M.H. & Glazer, A.N. (1982) Cyanobacterial phycobilisomes. Role of the linker polypeptides in the assembly of phycocyanin. *The Journal of Biological Chemistry*, **257**, 3429–3433.
- Zavřel, T., Chmelík, D., Sinetova, M.A. & Červený, J. (2018) Spectrophotometric determination of phycobiliprotein content in cyanobacterium *Synechocystis*. *Journal of Visualized Experiments*, **139**, 58076.
- Zhao, L.S., Huokko, T., Wilson, S., Simpson, D.M., Wang, Q., Ruban, A.V. *et al.* (2020) Structural variability, coordination and adaptation of a native photosynthetic machinery. *Nature Plants*, **6**, 869–882.
- Zhao, L.S., Su, H.N., Li, K., Xie, B.B., Liu, L.N., Zhang, X.Y. *et al.* (2016) Supramolecular architecture of photosynthetic membrane in red algae in response to nitrogen starvation. *Biochimica et Biophysica Acta*, **1857**, 1751–1758.
- Zheng, L., Zhang, Z., Wang, H., Zheng, Z., Wang, J., Liu, H. *et al.* (2023) Cryo-EM and femtosecond spectroscopic studies provide mechanistic insight into the energy transfer in CpcL-phycobilisomes. *Nature Communications*, **14**, 3961.
- Zheng, L., Zheng, Z., Li, X., Wang, G., Zhang, K., Wei, P. *et al.* (2021) Structural insight into the mechanism of energy transfer in cyanobacterial phycobilisomes. *Nature Communications*, **12**, 5497.
- Zheng, W., Wuyun, Q., Li, Y., Zhang, C., Freddolino, P.L. & Zhang, Y. (2024) Improving deep learning protein monomer and complex structure prediction using DeepMSA2 with huge metagenomics data. *Nature Methods*, **21**, 279–289.